Ocean Acoustic Tomography: Single Slice and Moving Ship Experiments

by Bruce M. Howe and Peter F. Worcester*

Technical Report
APL-UW TR 9308
July 1994

*Original contains color plates: All DTIC reproductions will be in black and white.

*Scripps Institution of Oceanography, University of California, San Diego

DISCLAIMER NOTICE

THIS DOCUMENT IS BEST QUALITY AVAILABLE. THE COPY FURNISHED TO DTIC CONTAINED A SIGNIFICANT NUMBER OF COLOR PAGES WHICH DO NOT REPRODUCE LEGIBLY ON BLACK AND WHITE MICROFICHE.

Ocean Acoustic Tomography: Single Slice and Moving Ship Experiments

by Bruce M. Howe and Peter F. Worcester*

Technical Report
APL-UW TR 9308
July 1994

Applied Physics Laboratory University of Washington
1013 NE 40th Street Seattle, Washington 98105-6698

*Scripps Institution of Oceanography, University of California, San Diego

ACKNOWLEDGMENTS

In addition to the authors, the principals in this work were K. Metzger and T. Birdsall at the University of Michigan (UM); B. Cornuelle, R. Davis, R. Knox, and W. Munk at the Scripps Institution of Oceanography (SIO); and J. Mercer and R. Spindel at the Applied Physics Laboratory, University of Washington (APL-UW). This report is intended to summarize the work of the entire group.

Many people helped collect and analyze the data for this project. We thank the technicians and ship crews who participated in the seven field trips: SVLA, VAST, Slice89, May88, MST88, MST89, and AMODE-MST. T. Duda at the Woods Hole Oceanographic Institution (WHOI) and S. Flatté at the University of California, Santa Cruz, participated in the analysis of Slice89 data. J. Boyd (NRL-SSC) helped obtain much of the environmental data. We acknowledge the dedication of many contributors at the institutions of the principal investigators. At APL-UW are K. Bader, B. Bell, M. Bolstad, A. Brooks, W. Eastman, W. Gropper, K. Kientz, S. Leach, A. Marshall, P. McKeown, L. Nielson, W. Nodland, R. Odom, L. Olson, B. Paisley, D. Reddaway, R. Stein, C. Walter, and E. Winkelman. At SIO are S. Abbott, K. Hardy, D. Horwitt, B. Ma, D. Peckham, P. and P. Russo, and R. Truesdale. At UM are J. Dawes and M. Dzieciuch. Also assisting were P. Boutin, J. Kemp, and S. Liberatore at WHOI and W. Fanning at the University of Rhode Island.

The work in the Greenland Sea was coordinated with a tomography experiment funded by the National Science Foundation and the Office of Naval Research.

Primary support came from the Office of Naval Technology and the Office of Naval Research (ONR Contracts N00014-87-K-0760, N00014-87-K-0120, N00014-91-J-4055, and N00014-91-J-4117). Secondary support came from NOAA (through SPAWAR contract N00039-91-C-0072).

ABSTRACT

The results of the ocean acoustic tomography work that supported the development of matched field processing (MFP) are summarized. This report focuses on two experiments. In Slice89 a single source transmitted to a vertical hydrophone array. This experiment improved our understanding of the single slice transfer function from scales of internal waves to 1000 km. It demonstrated the importance of unresolved high wavenumber ocean mesoscale variability to acoustic propagation. Any coherent signal processing technique must be robust against both internal wave variability and unresolved high wavenumber mesoscale variability, as both contribute roughly comparable amounts of travel time variance. The Acoustic Mid-Ocean Dynamics Experiment - Moving Ship Tomography Experiment (AMODE-MST) was a large mapping effort to address the primary goal of this tomography effort—to determine the precision with which the ocean mesoscale sound speed field can be measured for input into matched field (or other) processing of long-range acoustic transmissions. The experiment demonstrated that tomographic techniques can be used to measure the sound speed structure over a large area with high resolution.

TABLE OF CONTENTS

LIST OF FIGURES

LIST OF SYMBOLS AND ABBREVIATIONS

AMODE	Acoustic Mid-Ocean Dynamics Experiment
ATOC	Acoustic Thermometry of Ocean Climate
AXBT	Air Expendable Bathythermograph
CTD	Conductivity, Temperature, and Depth
FNOC	Fleet Numerical Oceanography Center
LFA	Low Frequency Active
MDA	Multi-Dimensional Array
MFP	Matched Field Processing
MST	Moving Ship Tomography
SGD	Signal Gain Degradation
SSS	Sound Speed Structure
SVLA	Single Vertical Line Array
VAST	Various Acoustic Systems Test
XBT	Expendable Bathythermograph

1. INTRODUCTION

This work supports a form of ocean acoustic signal processing known as matched field processing (MFP). The basic idea in MFP is to correlate measured hydrophone signals with predicted replica signals to determine parameters of interest, typically source location. In this process an accurate specification of the ocean sound speed field is crucial in generating the replica signals. If the sound speed field used differs too much from the true sound speed field, correlation will be degraded. The medium must be well known to obtain high, coherent gain in signal processing.

A simple example is useful. Consider a 20 Hz signal with a period of 50 ms and a wavelength of 75 m. To achieve coherent gain, the medium must be known well enough that relative phase errors in the predicted replicas are less than $\pi/2$, 12.5 ms or 18.75 m. This requirement is relaxed proportionally as one goes to lower frequencies. Typical ocean eddies can affect travel times by 10 ms to 100 ms over ranges of 100 km to 1000 km. Travel time changes associated with strong ocean features such as the Gulf Stream are on the order of 1 s. Thus, it is necessary to explicitly measure and take into account the ocean mesoscale and larger scales (order 100 km and larger). Furthermore, the technique must be robust against smaller (unmeasurable) scales, especially internal waves.

Recently, satellite infrared imagery and altimetry have been used to infer the subsurface sound speed structure. The temporal and spatial coverage is not always adequate, however, and inferring subsurface ocean sound speed structure from surface measurements alone is not without errors. This is particularly so during summer, when the warm, shallow thermocline masks deeper ocean structures in satellite infrared imagery.

The tomographic approach is an alternative source of subsurface data: there is a nominal n^2 growth of data with the number of instruments used; large areas can be sampled; and it is inherently an acoustic measurement, so the resulting sound speed fields should be well suited for subsequent use in a high gain acoustic system. To obtain high spatial resolution, a moving source and/or receiver can be used to supplement fixed instruments. This is the main idea we have pursued in this work.

In the future, estimates of sound speed structure over large volumes would almost certainly come from the Fleet Numerical Oceanography Center (FNOC). The Center will be routinely using IR, altimeter, and XBT data as available, combined with time dependent ocean models; any tomographic data being collected would also be used by FNOC in its products.

The tomography data were not intended to replace the conventional measurements used in conducting precise propagation experiments using MFP. Rather, the tomography effort was seen as a stand-alone project that would make use of the conventional environmental measurements for comparison purposes.

2. BACKGROUND

2.1 Determining the Ocean Sound Speed Field

There are many ways to measure and infer the sound speed structure within the ocean. The most precise way to determine the sound speed at a point is to measure temperature and salinity using a CTD (conductivity, temperature and depth) instrument and then employ the (empirical) equation of state. The most common operational method, however, is to measure profiles of temperature using (less accurate) expendable bathythermographs (XBTs), infer salinity from historical data, and then calculate sound speed. Other instruments that produce in situ information related to the sound speed field include inverted echosounders (single path reflection tomography), and moored and drifting buoys with various sensors. These methods are difficult to use operationally because of the poor spatial sampling and the cost (including the measurement platform).

Subsurface ocean structure can also be inferred from satellite infrared imagery, using feature models for fronts, rings, and eddies. Or, satellite altimetry combined with geostrophy can be employed to infer the subsurface density field. Also, instruments that measure currents directly (current meters, horizontal electric field sensors that measure the barotropic current components, expendable current profilers, to name a few) can obtain data that are then combined with models to yield estimates of density, and thus temperature, salinity, and sound speed, via historical temperature-salinity relations and the equation of state. Acoustic tomography is yet another method for obtaining data about the ocean interior.

Nevertheless, there will always be a paucity of data. It may never be possible to directly measure the sound speed field as well as one would like; one will rely on the physics in numerical ocean models to provide the temporal and spatial interpolation and extrapolation. This is an area of very active research. In many ways, the problem is similar to numerical weather forecasting. For the ocean, though, the time scales are longer, the space scales are smaller, and the data are relatively sparse. The trend in data assimilation work is toward 4-D assimilation, using all the data over some finite period of time (several weeks or months in the ocean case) to calculate the best nowcast and then the best forecast.

How precisely must we know the sound speed field for successful matched field processing? This question is still largely unanswered. The answer clearly depends on what acoustic frequencies are of interest. It also depends on the frequency wavenumber spectrum of ocean variability. For the purposes of these experiments though, we have attempted to measure the sound speed as accurately as feasible. The ocean spectrum is still not well understood or known. For instance, in the deep ocean we know there can be 0.1°C (0.3 m/s) changes over a year, but we don't know the spatial and temporal scales.

Errors in mapped fields of ocean variables arise from measurement error, sampling error, and geophysical sources. Measurement error includes both random and bias errors; it can also include the statistical errors in converting from, say, sea surface height to interior sound speed. Sampling error includes errors due both to temporal and spatial aliasing. Geophysical errors include such effects as high frequency variability (e.g., internal waves).

2.2 Principles of Ocean Acoustic Tomography

By measuring the travel time of an acoustic pulse over a known range through the ocean, one can infer the propagation speed of sound along the path. By measuring travel times along reciprocal paths, one can infer current velocity along the path because sound travels faster with a current than against one. Tomography consists of taking many such measurements and using rigorous inverse methods to obtain the sound speed (and current) field. This is shown schematically in Figure 1. A 3-D picture of typical instruments is shown in Figure 2. We emphasize several key points about tomography: each datum is an integral or average along a path, a multitude of crossing paths is necessary for a good reconstruction of the field, and the number of data grows roughly as the square of the number of instruments (as opposed to a linear growth for point measurements). The seminal paper on ocean acoustic tomography is by Munk and Wunsch (1979); a recent review is by Worcester et al. (1991).

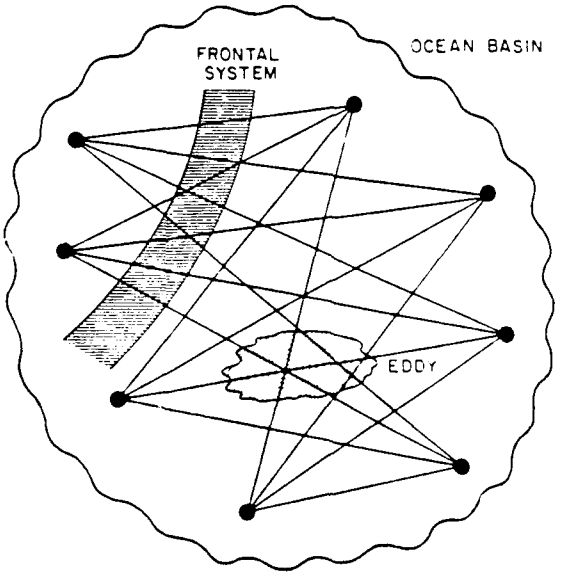

Figure 1. Acoustic paths going through eddies and fronts. Data from a multitude of such paths crossing at many different angles can be used to reconstruct the field.

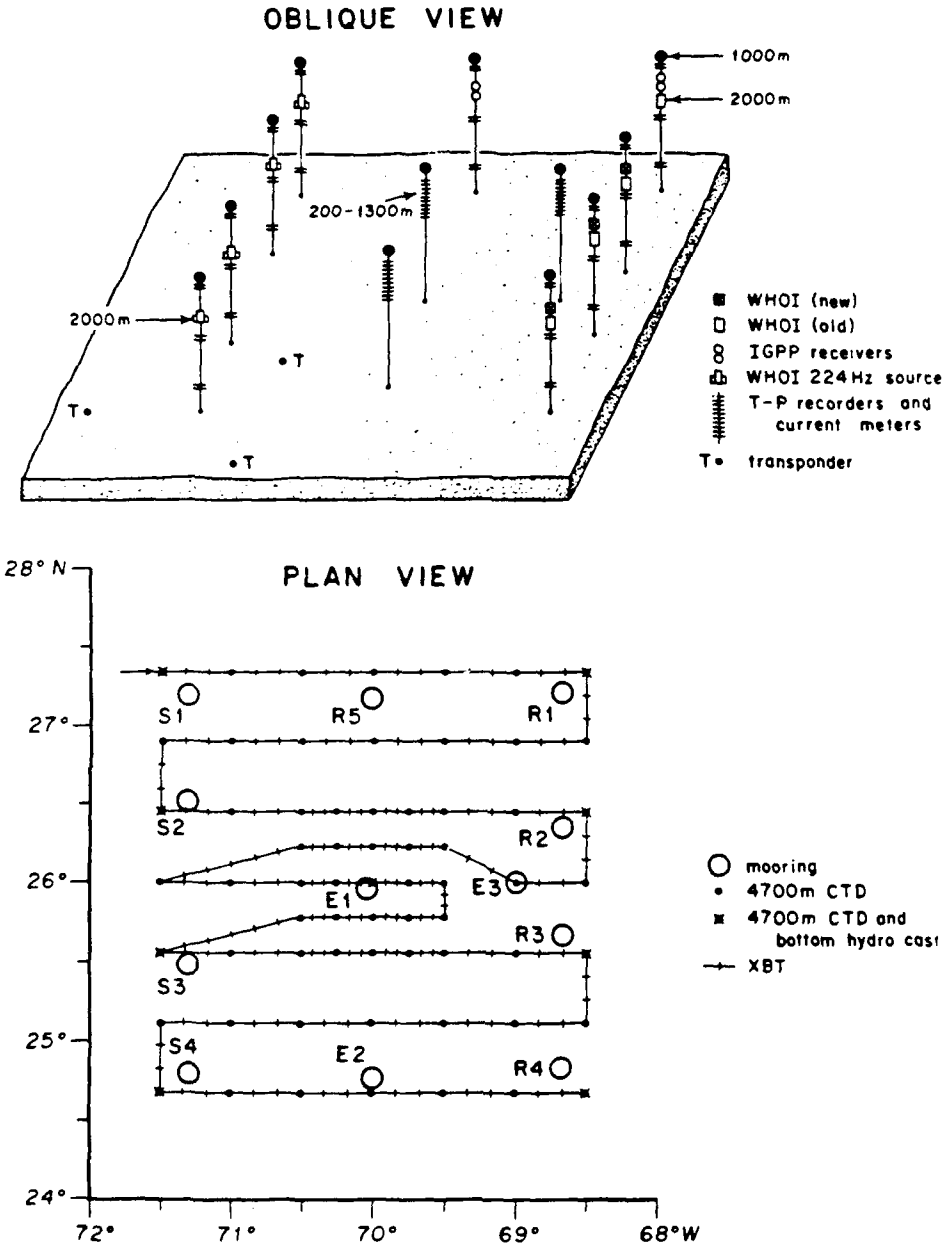

Figure 2. A 3-D picture of the 1981 tomography experiment showing moorings and tracking transponders.

One can approach a discussion of ocean acoustic tomography at three levels of sophistication: they can be called horizontal, vertical, and loop-harmonic tomography, respectively. The first two were described by Munk and Wunsch (1979), the third by Cornuelle and Howe (1987). The magnitude of expected travel time signals can also be ranked in a similar way: horizontal ocean variability produces the largest travel time signal, followed by variability in the vertical, and lastly, by horizontal variability nominally at convergence zone spacing.

Horizontal tomography assumes straight rays; it is this version that is analogous to the medical CAT scan. The fundamental theorem involved is the projection slice theorem, Figure 3 (Kak and Slaney, 1988). The projection through the medium of interest taken at some angle θ in physical space corresponds to a line at angle θ in Fourier space (the spatial wavenumber domain). Thus, to map physical space unambiguously, projections at many different angles need to be measured to fill in Fourier space.

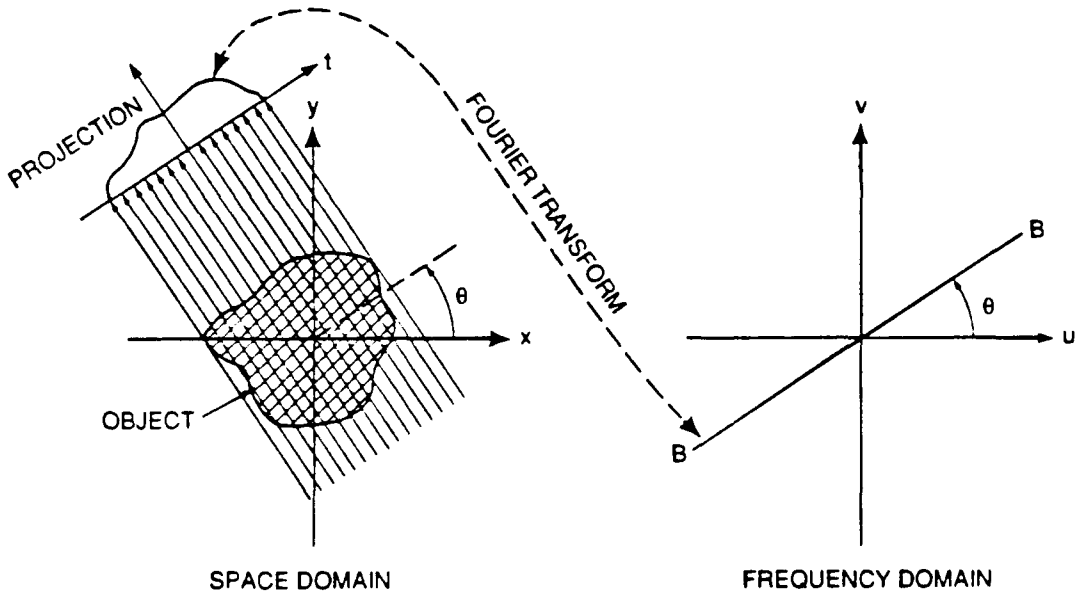

Figure 3. Projection slice theorem. A projection at angle θ maps into a line in Fourier space at angle θ. (after Kak and Slaney, 1988)

The second level of sophistication looks at sound propagation in the ocean waveguide in more detail to obtain vertical resolution. In the ocean the temperature decreases with depth while the pressure increases with depth. Because the speed of sound increases with both temperature and pressure, there is a minimum in sound speed, typically at 1000 m. Sound propagates along quasi-sinusoidal ray paths which turn at different upper and lower turning depths, depending on the launch angle, Figure 4. This

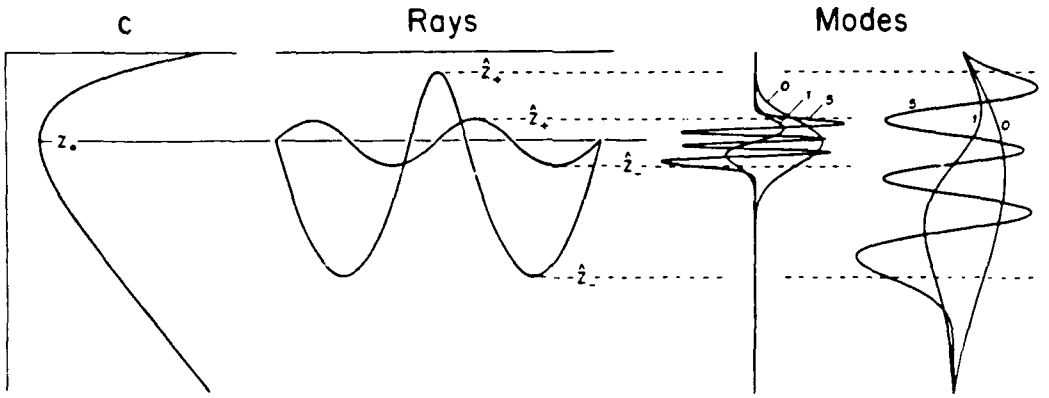

Figure 4. A typical ocean sound speed profile is shown with acoustic rays. Rays with differing launch angles sample different depths. The equivalent acoustic mode representation is shown also.

fact, that different rays have different turning depths, is used to obtain depth-dependent sound speed. A sound speed perturbation at shallow depth will affect only those rays traversing that depth; rays that turn deeper will remain unaffected, Figure 5.

At the third level, loop harmonics, we use the fact that because the rays are quasi-periodic in range they sample the upper ocean (which has the most variability) in a quasi-periodic way. This sampling in range looks like a comb function, Figure 6, and the Fourier transform of a comb function is a comb function in the wavenumber domain. If

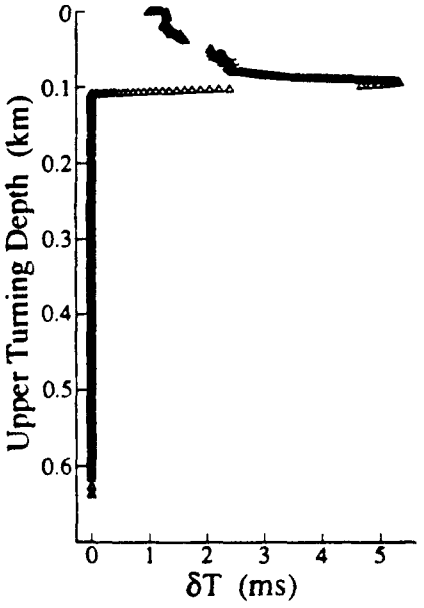

Figure 5.

Travel time anomalies computed for a sound speed perturbation with an amplitude of −1 m/s at 100 m depth, linearly decreasing to zero at 90 and 110 m. The range is 1000 km. (from Cornuelle et al., 1993)

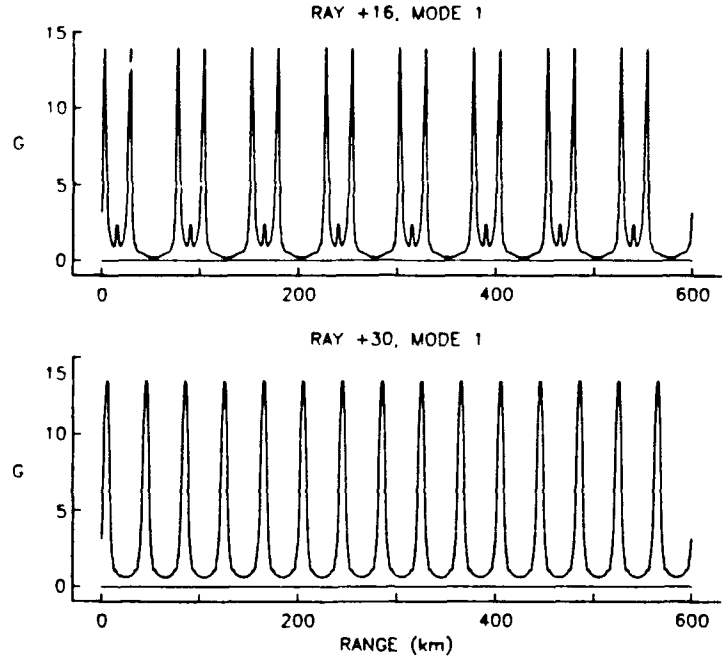

Figure 6. Comb sampling function of a ray as a function of range for a first baroclinic mode. Ray +16 leaves the source with a positive launch angle and has 16 upper and lower turning points. Ray +30 leaves the source with a positive launch angle and has 30 turning points. Ray +16 has shallow and deep turning points and samples most of the water column, whereas the Ray +30 samples only the main thermocline. The first baroclinic mode has one nonzero peak in the main thermocline between 300 m and 1000 m and is zero elsewhere. The ordinate G is the integral of the mode function along the ray path. G is positive as the rays go through the main thermocline and is zero when the ray is above (as is the case for Ray +16) or below the main thermocline. (from Cornuelle and Howe, 1987)

rays with different nominal wavelengths are present, the wavenumber spectrum can be filled in, and resolution obtained. Resolution is the ratio of the expected error variance of a model parameter after the information in the data is used to the error variance of the model parameter in the absence of data, the *a priori* variance. An example of a resolution spectrum from a simulation is shown in Figure 7. If travel times along enough different rays with similar turning depths are measured (by using vertical arrays of hydrophones and/or transmitters) one can unambiguously determine the location of features with scales shorter than the ray double loop length. This is because some rays will go through a "short" feature and others will not. Conversely, all rays will be affected about the same

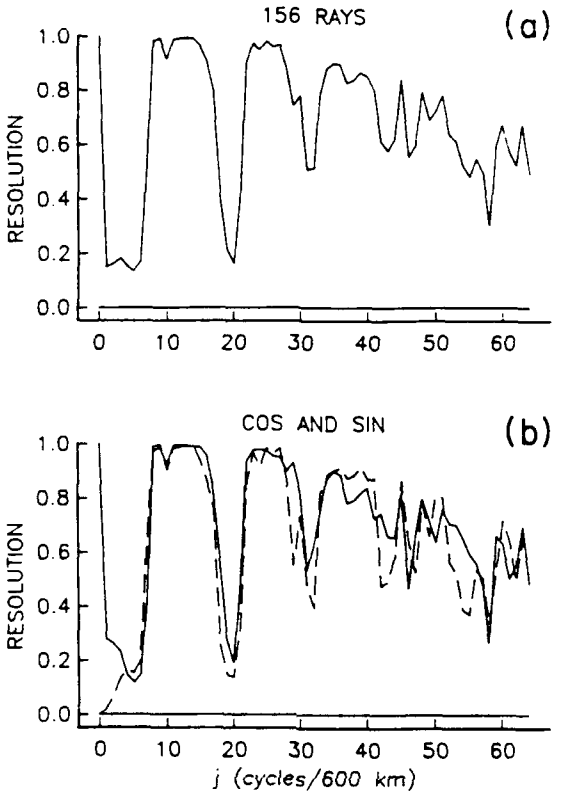

Figure 7. The resolution spectrum showing good resolution of the mean and at wavenumbers corresponding to double loop wavenumbers and their harmonics. (a) the total resolution using 156 rays in a 600 km domain, and (b) the cosine and sine components of the resolution spectrum. (from Cornuelle and Howe, 1987)

by large features, and they will be indistinguishable from the mean. An example in physical space from a simulation is shown in Figure 8. The high wavenumber features are resolved, while the low wavenumber features are not (and are lumped in with the mean, which is well resolved). Thus one can, given sufficient signal-to-noise ratio, determine high wavenumber components of the field, as well as the mean, as a function of depth.

In all three cases, least-squares techniques have been used to invert data for the fields of interest. These techniques are also called stochastic inversion, objective mapping, and weighted, tapered, least-squares, to name a few. The method is described by Cornuelle et al. (1993) and Howe et al. (1987). There is some nonlinearity involved because the acoustic paths in the estimated and/or true ocean are not the same as in the assumed reference state. To date, simple iteration appears adequate to resolve this problem, provided that care is used in constructing the reference sound speed field required by least-squares techniques.

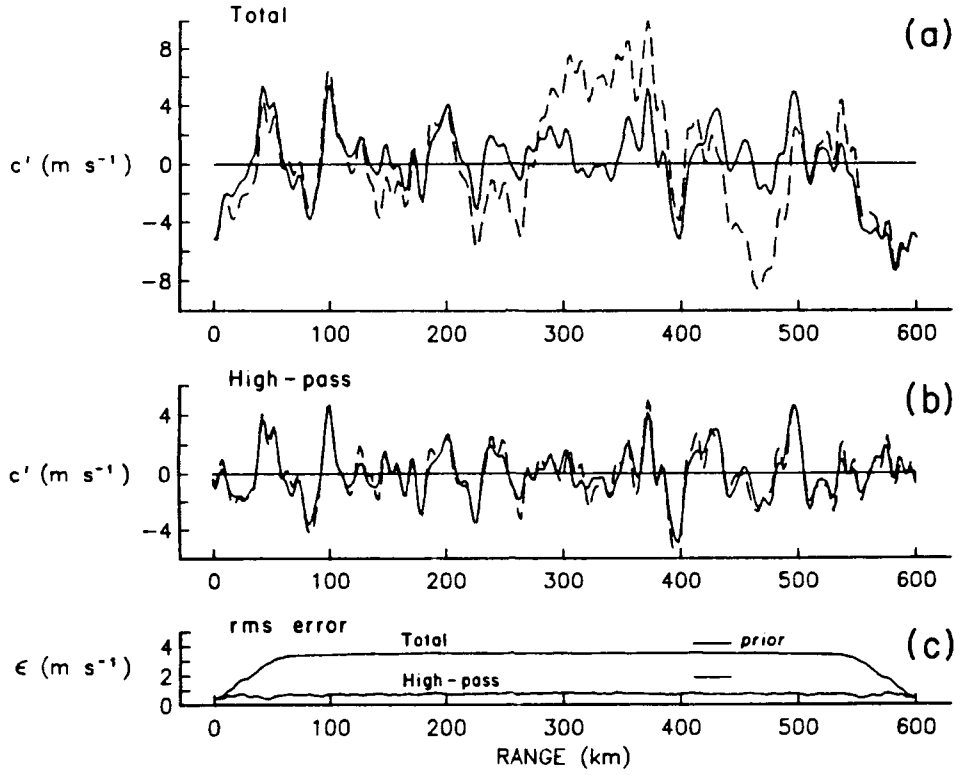

Figure 8. A simulation showing the total and high wavenumber sound speed at 1000 m, both the true values (dashed) and the reconstructed ones (solid). The estimated rms errors are shown at the bottom. (These are not the difference between true and estimated, rather they are estimated as part of the least-squares inverse procedure). The horizontal lines labeled "prior" indicate the expected errors in the absence of data for the total and high-pass sound speed. The difference between the prior errors and the errors estimated with data is indicative of the information in the data. (from Cornuelle and Howe, 1987)

3. SINGLE SLICE EXPERIMENTS

Two single slice experiments were conducted to better understand the effects of ocean sound speed perturbations on acoustic propagation. The first one, the Single Vertical Line Array (SVLA) Experiment, for the first time observed acoustic time fronts sweeping across a vertical receiving array. The second one, the 1989 single slice tomography experiment (Slice89), was able to quantify both internal wave effects and larger scale effects at the mean wavenumber and at wavenumbers corresponding to ray loop harmonics. The geographical locations of these experiments is shown in Figure 9.

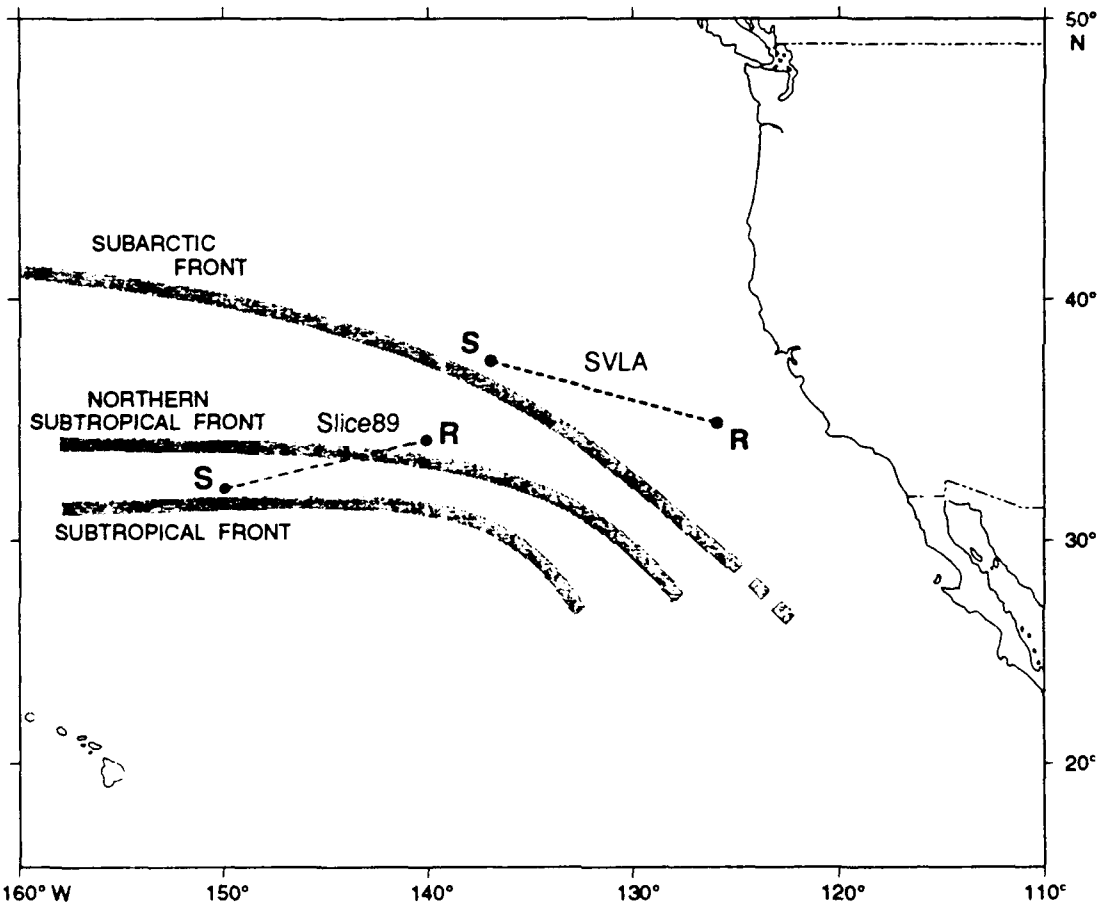

Figure 9. Geographical area of the SVLA and Slice89 experiments. The distance between the sources (S) and the receiving arrays (R) is approximately 1000 km for both experiments. Note that the SVLA source position is close to the Subarctic Front but otherwise the water mass between source and receiving array is relatively homogeneous, while the Slice89 path crosses the northern subtropical front. (modified from Lynn, 1986)

3.1 Single Vertical Line Array (SVLA) Experiment

As one part of the SVLA experiment, an 80 Hz source transmitted to a receiving array over a distance of 1000 km. The tomography aspects of this experiment are described by Sparrock (1990) and illustrated in Figures 10 and 11. There are several limiting aspects of the experiment that should be noted. The source was suspended at 150 m and transmitted a 50 ms wide pulse; the receiving array covered only the depth range 400 m to 1300 m. The accuracy of the positioning of the instruments was marginal.

Because of the aspects mentioned above, it was not possible to extract quantitative information about the ocean sound speed field from the data; but SVLA did show that in a more controlled experiment (such as Slice89 described below) one could expect to obtain a wealth of information and greater insight into the details of acoustic propagation along a single slice.

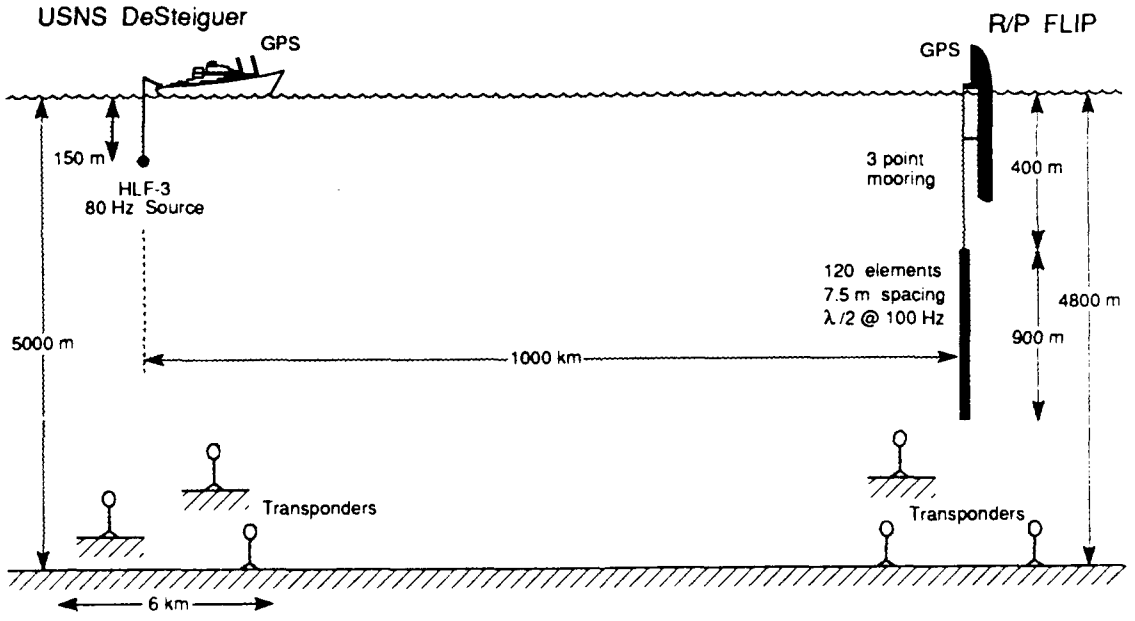

Figure 10. Summary of the SVLA experiment geometry. (from Sparrock 1990)

3.2 The Slice89 Experiment

Slice89 was conducted as one part of the VAST experiment. The geographical location is shown in Figure 9 and the experiment geometry in Figure 12.

The limitations of the SVLA experiment were largely eliminated, and it was possible to extract useful information about the ocean sound speed field from the acoustic data. The range between the source and receiver was 1000 km. The source was moored

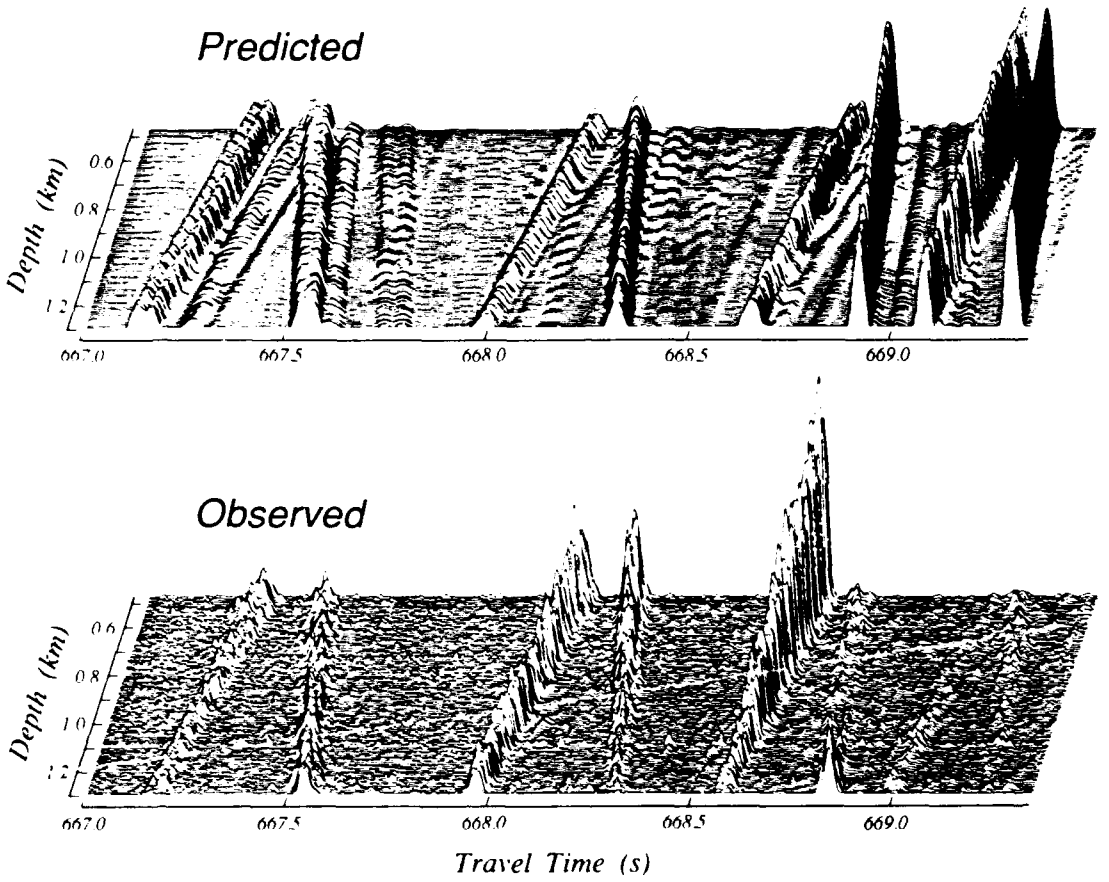

Figure 11. Measured arrival patterns and predictions made using the WKBJ range-independent code of Brown (1982). There are several features that can be observed: the overall wavefront structure is well predicted: there are fluctuations in the measurements not in the predictions; and the amplitudes are predicted only fairly. These results were not unexpected, but nevertheless represent a major experimental confirmation of our qualitative understanding of the problem. (from Sparrock 1990)

near the sound channel axis (800 m) and transmitted at 250 Hz with a 12 ms wide pulse. The vertical receiving array spanned the water column between the surface and 3000 m, and the instruments were positioned to approximately 2 m relative, and 100 m absolute. Extensive AXBT, XBT, and CTD data were collected along the slice.

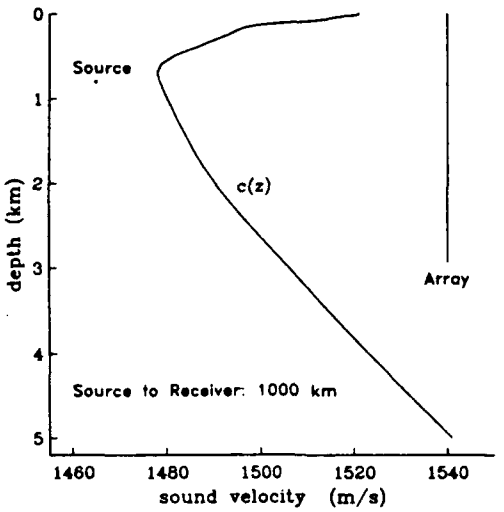

Figure 12. Summary of the Slice89 experiment geometry. (from Duda et al., 1992)

The following discussion of the results is divided into two parts: internal wave aspects and tomography aspects. First, though, we show measured and predicted arrival patterns in Figures 13 and 14. The agreement between measured and predicted time fronts is excellent for most of the pattern; only in the last second of the pattern is the measured pattern somewhat broader on each side of the sound speed axis than the predicted pattern. This difference, which will be discussed below, is believed to result from internal waves scattering the axial energy. Deviations of the measurements over times less than a day are attributable to internal waves. Deviations over longer times are attributed to ocean (geostrophic) eddies.

3.2.1 Internal Waves

The main questions we wanted to answer were

1. What are the temporal and spatial (vertical) correlation functions of the time fronts?
2. How do measured correlations compare with predictions?

The first question has been addressed by Duda et al. (1992), and their conclusions are summarized here. The second question is addressed by Colosi et al. (1994).

The time fronts (pressure amplitude versus travel time and depth) have already been shown in Figures 13 and 14. Three distinct fluctuation signals were observed. The first signal, wave-front displacement and rotation, had time scales longer than a few hours, with a dominant period of about 12 h, and was well fit with a straight line in the vertical

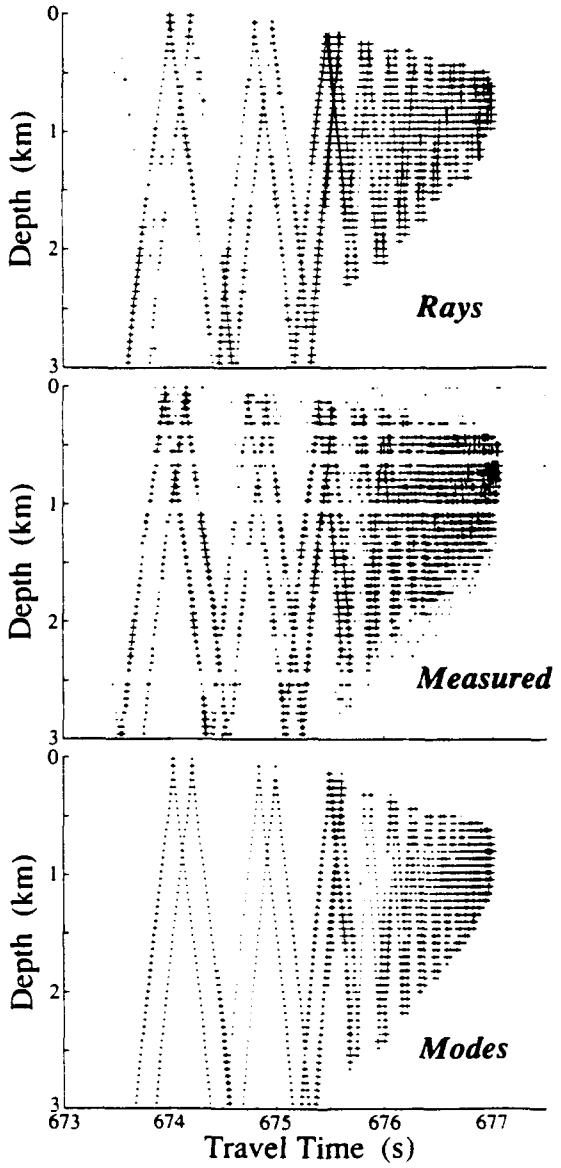

Figure 13. (top) Predicted travel times versus hydrophone depth computed using a range-dependent ray tracing code and the sound speed field obtained by objectively mapping all of the CTD, XBT, and AXBT data obtained during the experiment. Only peaks with intensities within 40 dB of the maximum are shown. Although the symbol sizes are proportional to peak intensity in decibels, the intensities calculated from the ray trace are not reliable. (middle) Measured pulse travel time versus hydrophone depth for the signal transmitted on yearday 192, 1989, at 19:20 UTC. Only peaks with signal-to-noise ratios above 10 dB are shown. Symbol size is proportional to intensity in decibels. (bottom) Predicted travel times versus hydrophone depth computed using a range-independent broadband normal mode calculation. The sound speed field was the average of the objective map of all the CTD, XBT, and AXBT data. Only peaks with signal-to-noise ratios within 30 dB of the maximum are shown. Symbol size is proportional to intensity in decibels. (from Worcester et al., 1993)

along each wave-front segment. This signal corresponded to the along-range compression/expansion of the accordion-like pulse, or equivalently to relative displacements of the wave-front vertices. The compression of the entire 2000 ms long wave front had a peak value of about 20 ms, Figure 15.

A *second signal, intermediate-scale distortion*, also had time scales longer than a few hours but had vertical correlation scales between 60 m and 1 km. The contribution of this signal to the total travel time variance was only about 2 ms^2, consistent with expectations from internal wave effects, Figure 16.

The third signal, broadband fluctuations, was vertically uncorrelated over the 60 m hydrophone spacing and temporally independent at the smallest available time lag of 10 min. The variance of this signal was between 25 ms^2 and 50 ms^2, Figu · 17. These fluctuations may be due to wave-front instabilities; wave fronts were occasionally observed to have broken into microfronts. A detailed study of the microfronts was not possible given the temporal and spatial sampling, so this link is only speculative.

In summary, fluctuations were observed at all resolvable temporal and spatial scales. Fluctuations unresolved by the 10 min and 60 m hydrophone spacing were greater than 5 ms rms. Wave front displacements independent of depth contributed about 3 ms rms, dominated by internal tides. Other curved wave front distortions with time scales longer than a few hours contributed 1 to 2 ms rms.

Colosi (1993) and Colosi et al. (1994) discuss the effects of internal waves on the last second of the arrival pattern and compare the data with predictions.

3.2.2 Tomography Analysis

One of the main goals of Slice89 was to experimentally verify the theory proposed by Cornuelle and Howe (1987). This theory (Section 2.2), predicts that acoustic data are sensitive to high ocean wavenumbers and that the latter can be obtained from the former. Unfortunately, the associated environmental data were inadequate to do this directly; however, indirect evidence supports the theory. Detailed results are presented by Worcester et al. (1994) and Cornuelle et al. (1993).

The agreement of the measured acoustic travel times with those predicted using objectively mapped sound speed fields based on profile data has already been shown (Figure 13). Although the overall agreement between measured and predicted travel times was quite good (some exceptions were noted in 3.2), there are still differences between the two. It is in fact these small differences that can provide more information about the state of the ocean sound speed structure. Perturbation travel times (measured minus predicted) for various time periods and averages are plotted in Figure 18. Additional plots of travel times versus time (not shown) indicate that there is no low frequency trend in the data and a simple average over time is acceptable. Perturbation

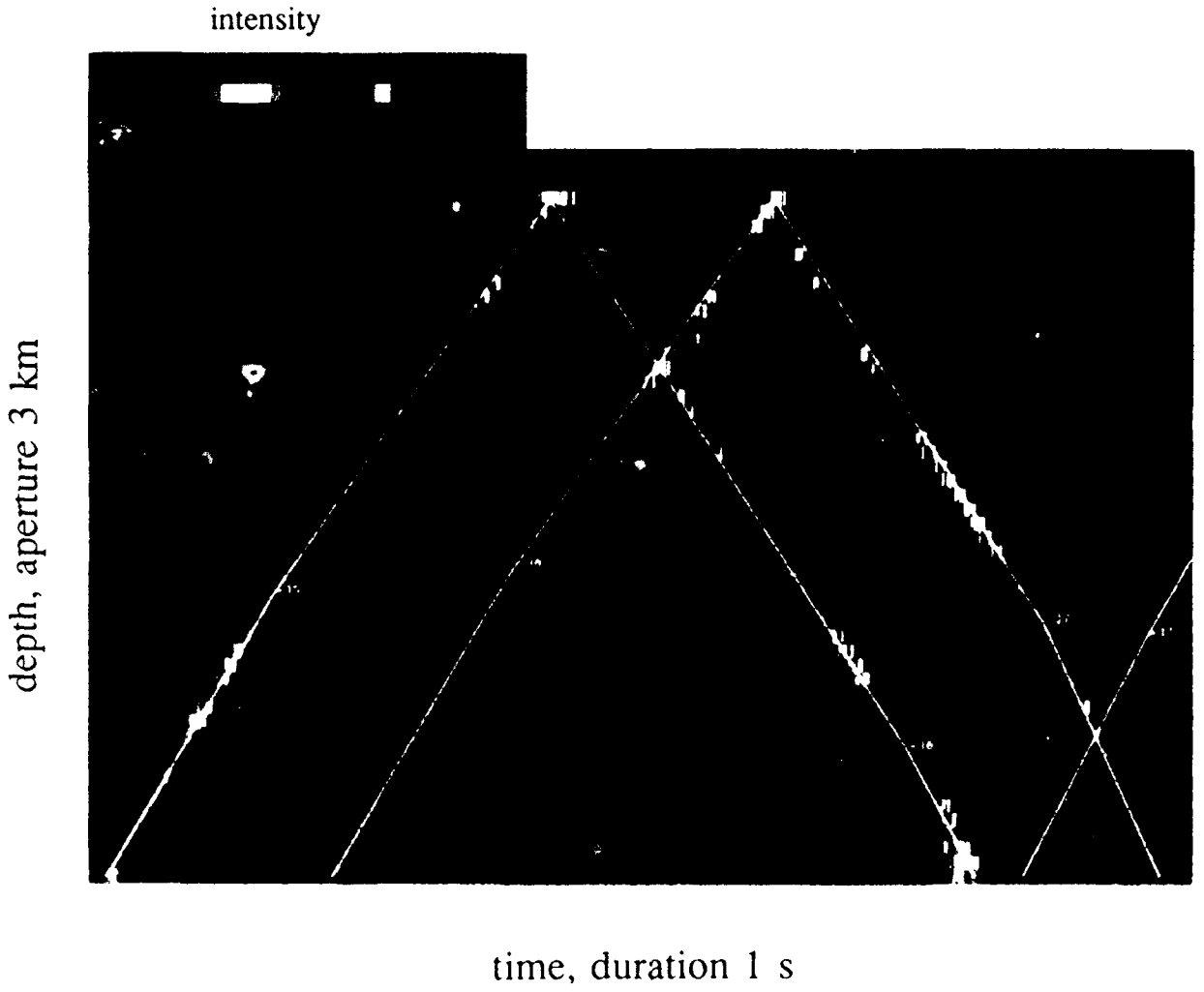

Figure 14 An expanded portion of the arrival pattern in travel time, depth space. The lines and ray identifiers are part of a tracking/editing program used to associate measured peaks with predicted ray arrivals (from Duda et al., 1992)

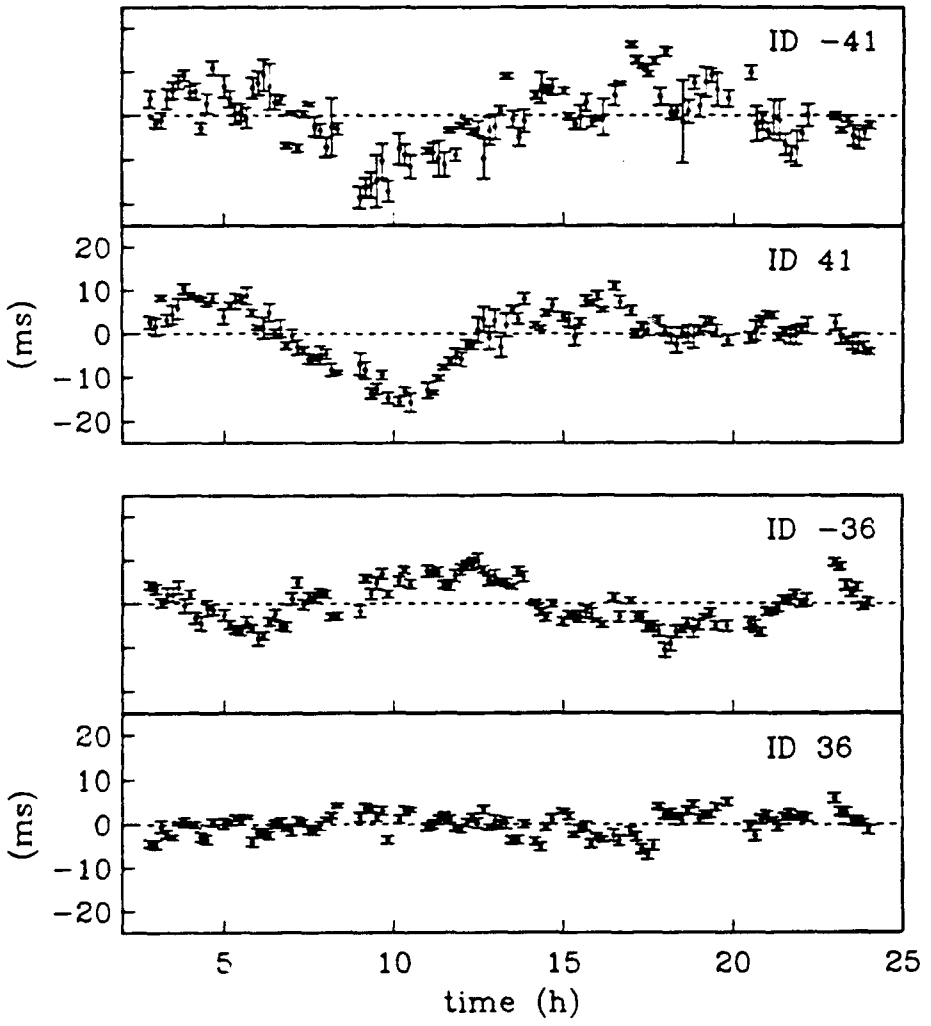

Figure 15. Four examples of wave-front displacement as a function of time. (Ray -41 leaves the source with a negative angle and has 41 turning points; thus there is an "extra" lower loop. Ray +36 leaves the source with a positive angle and has an equal number of upper and lower turning points.) Effects near the semidiurnal tidal period are clearly seen. The confidence intervals reflect the number of vertically spaced samples included in the displacement calculation. (from Duda et al., 1992)

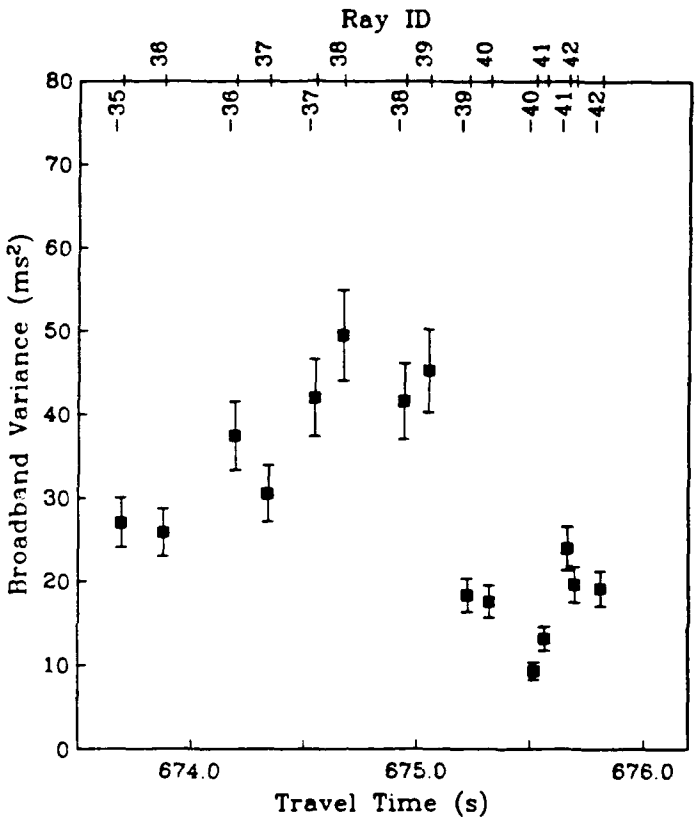

Figure 17. Variance of the broadband fluctuations, averaged over depth and time, calculated after subtraction of the best-fit linear wavefronts for each ray ID and for each 10-minute sample. The broadband fluctuations contain more than half of the total variances. (from Duda et al., 1992)

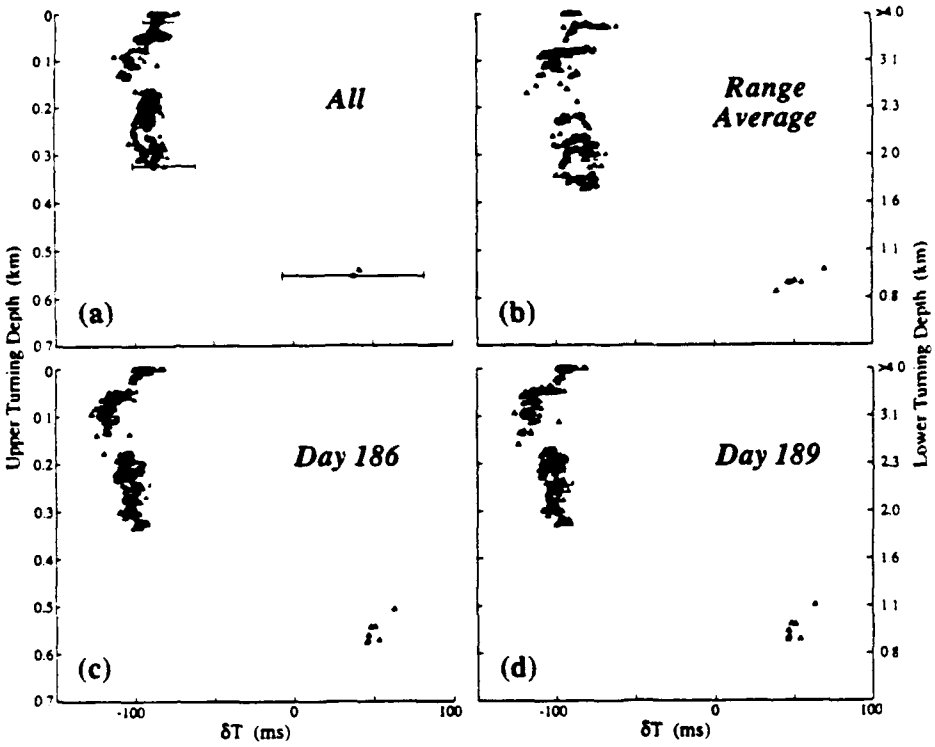

Figure 18. Travel time anomalies computed by subtracting the predicted travel times (calculated with a range-dependent ray trace using a variety of reference states) from the mean measured travel times (calculated by averaging over all of the acoustic data) plotted as a function of ray upper turning depth. (Corresponding lower turning depths are indicated on the right-hand side of the figure). The predictions were made with four different sound speed fields: range-dependent objective maps combining all of the CTD, XBT, and AXBT data, (top left); using data from day 186 only (bottom left); using data from day 189 only (bottom right); and a range-independent sound speed profile constructed by range-averaging the objective map combining all of the CTD, XBT, and AXBT data (top right). The number of rays with near-axial upper turning depths varies from case to case because predictions for the nearly horizontal ray paths are sensitive to the details of the sound speed profile. The number of rays successfully identified therefore varies from case to case. (from Worcester et al., 1994)

travel times for rays that turn at the same depth were about 25 ms peak-to-peak (the horizontal breadth of the scatter), large compared to the expected measurement precision of 2 ms rms for a 1 day average. These differences are attributed to range dependence in the sound speed field that is not resolved by direct profile measurements. Furthermore, there is a gross variation of about 50 ms as the depth increases from 0 to 400 m, and a 150 ms difference between the well-resolved ray travel times and the axial travel times, indicating that the depth dependence of the range averaged reference field is in error. The (large) 100 ms offset of the data is attributed to uncertainty in the absolute range between the source and receiving array.

These travel time differences, or anomalies, are inverted to obtain a range dependent sound speed field, Figure 19. [See Cornuelle et al. (1993) for important details of how this is done.] Inversions were done using as a reference field both the simple average of all the profile data (for practical purposes, this is the same as the range-average profile used in Figure 18, top right) and the range-dependent field obtained by objectively mapping the profile data. Residual travel times (measured minus estimated through the estimated field) are about 2 ms rms, consistent with the *a priori* errors.*

The resolution as a function of horizontal scale can be quantified by plotting the fraction of *a priori* sound speed variance resolved by the various data as a function of horizontal (ocean) wavenumber, Figure 20. Although we restrict our attention here to mode 1 results, similar results are obtained for the higher modes. (The first oceanographic mode describes to a large extent the simple vertical motion of the main thermocline.) This is simply the transfer function between the measurements and the ocean. For just the profile data, the resolution steadily decreases with wavenumber and is 0.5 at 70 km wavelengths. [Even though spacing was nominally 25 km (Nyquist wavelength 50 km), measurement errors reduce the resolution.] For the inversion using only acoustic data, significant resolution is evident for wavelengths corresponding to the ray double loop lengths and the second harmonics (since the rays are distorted sinusoids). The mean, zero wavenumber, component is relatively poorly resolved due to its small expected variance (the error in the mean reference state based on the profile measurements is relatively small) and its ambiguity with long-wavelength components.

There is little overlap in resolution at high wavenumbers in the profile data and the acoustic data. Instead of comparing the two inversions (profile only and acoustic only), the two data sets can be combined together in a single inverse, in which inconsistencies are identified by large residuals in the least-squares fit. This has the added advantage of

*It must be mentioned that significant problems in doing the acoustic inversions resulted from using environmental profile data that had been combined at depth with the Navy's GDEM sound speed climatology data base. The acoustic data were inconsistent with this reference state. It was determined that GDEM has errors at depth: there are unphysical variations as a function of depth. The reasons for this were not investigated. The Levitus data base (1982) was found to be consistent with the data.

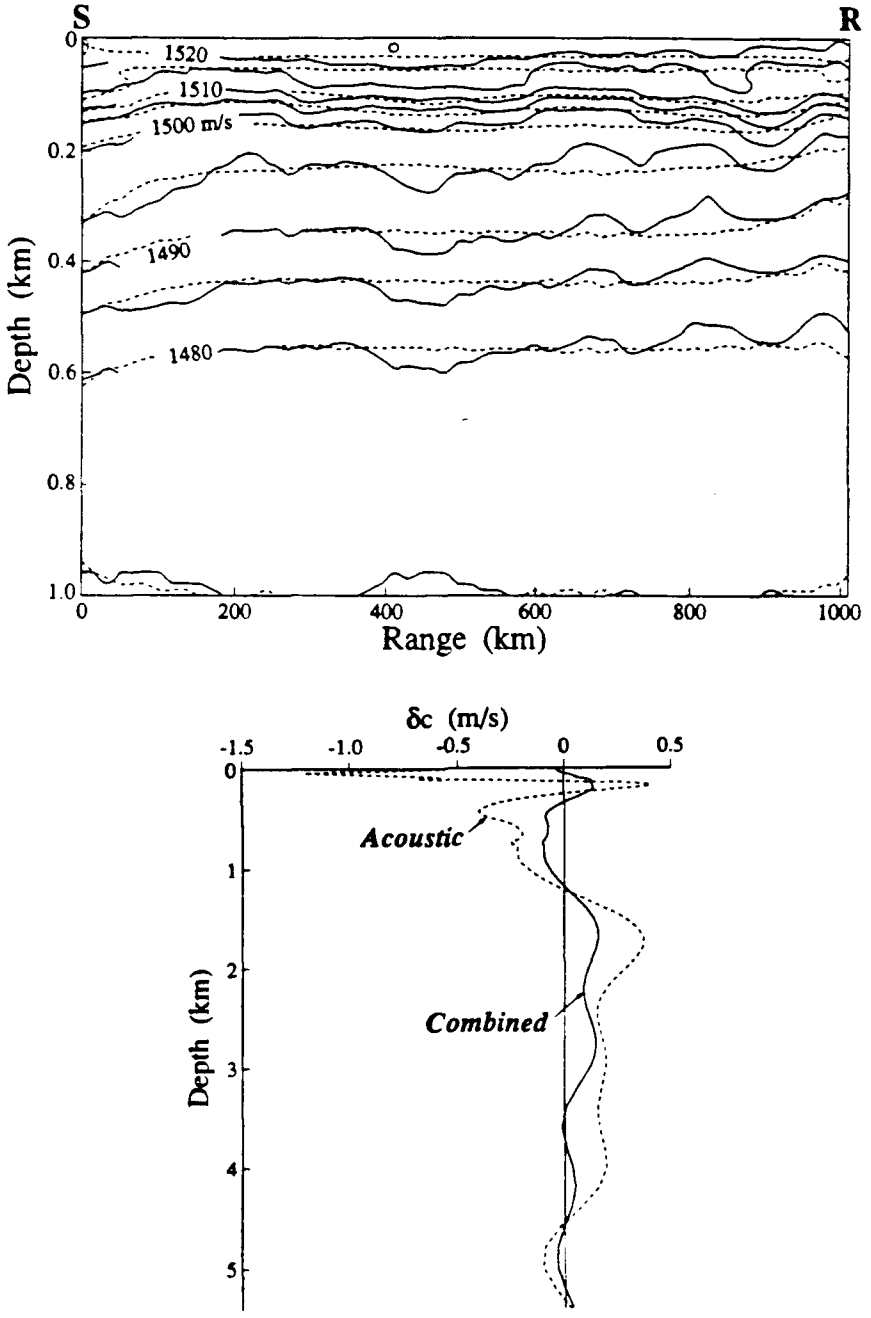

Figure 19. (top) Objectively mapped sound speed fields (m/s) obtained (i) by inverting the travel time data (dashed), and (ii) by inverting the combined data set consisting of the travel times and point measurements. Range is in kilometers from the source, which is on the left. (bottom) Range-average of the sound speed field computed from the acoustic travel times alone (dashed contours above) and from the combined data set (solid contours above) minus that computed from the CTD, XBT, and AXBT data alone.

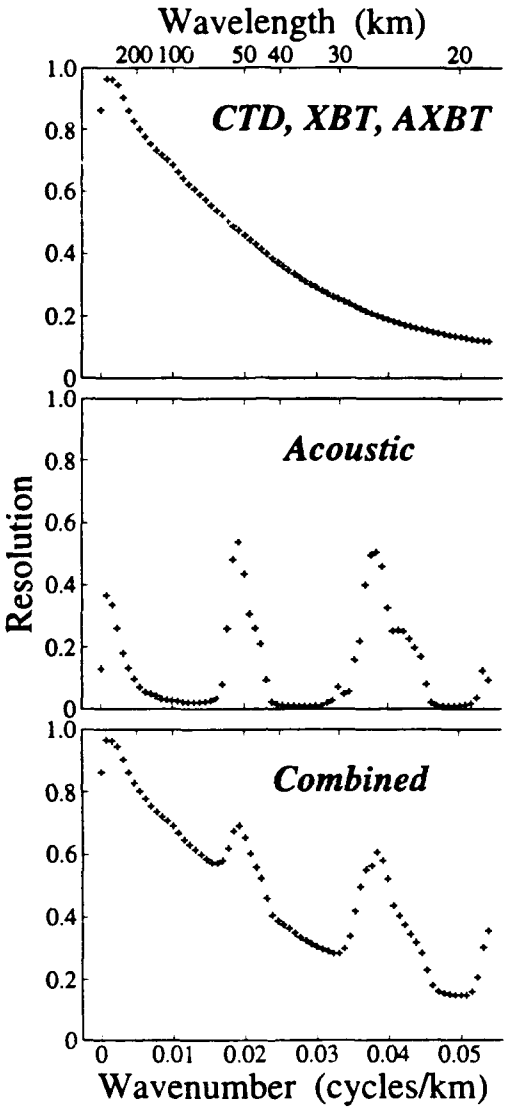

Figure 20. Fraction of the a priori sound speed variance in mode 1 resolved by the objective maps as a function of horizontal ocean wavenumber, for maps constructed combining all of the CTD, XBT, and AXBT data (top), combining all of the acoustic travel time data (middle), and for a joint objective map combining the CTD, XBT, AXBT, and acoustic travel time data (bottom). (from Cornuelle et al., 1993)

producing the best possible sound speed field. In practice, the inversion is done in a two-step process. First the profile data are fit, and then rays are traced in the resulting field, which is then improved using the acoustic data. This minimizes the nonlinearity of the acoustic forward problem by using the best available reference state. All data residuals were consistent with the *a priori* errors.

As a check on the linearization of the forward problem, the forward problem matrix made from the range-independent rays was compared with that made from the range-dependent rays used in the combined inverse. Changing the ray path may change the derivatives, particularly for the model parameters describing small-scale ocean perturbations. Figure 21 shows the rms average and the rms difference of the two matrices for mode 1. We take the latter to represent a measure of the nonlinearity arising from the displacement of ray paths caused by changes in the range-dependent sound speed field relative to the range-independent reference state. The rms difference is about 3% of the rms average for the lowest wavenumber, but rises to nearly 100% for the highest wavenumbers. The higher modes, with shorter vertical scales, have generally stronger nonlinearities. For example, for the zero wavenumber the nonlinearity is 3% for mode 1 and 8% for mode 2, increasing to 12% for mode 5. The peaks and valleys in the two curves result from the loop harmonic resonance described earlier. For the purposes of

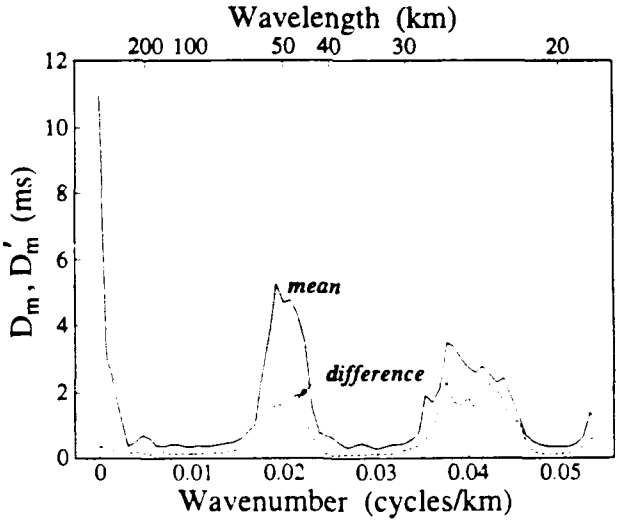

Figure 21. The forward problem matrix showing effects on nonlinearity. Solid curve: rms elements of the forward problem matrix for mode 1, averaged over all rays and over two reference states, the range-independent state, and the range-dependent objective map of all the data. The elements are plotted versus the horizontal wavenumber. Dashed curve: rms elements of the difference between the two forward problem matrices for mode 1, averaged over all rays in the data. (from Cornuelle et al., 1993)

the inverse, the nonlinearity only matters in the areas predicted to have significant horizontal resolution (in Figure 20); if the horizontal resolution at a particular scale is small, the inverse will not infer a sound speed perturbation at that scale.

This measure of nonlinearity is much more stringent than a simple calculation of travel time errors due to incorrect ray paths. It includes the effects of phase shifts in the ray paths, in which the horizontal locations of the upper turning points differ between the range-independent and the range-dependent rays. Range-dependent inversions that include high-wavenumber components depend on the detailed differences in the horizontal sampling properties of the ray paths. This single case suggests that resolution of high wavenumbers puts stronger requirements on the accuracy of the ray paths than resolution of low wavenumbers.

Lastly, inversions for the range-averaged sound speed profile were performed, using as a starting reference Levitus climatology. The purpose was to show that with iteration one could, if necessary, start from climatology rather than with in situ data. Results are consistent with those above and are not shown here; see Cornuelle et al. (1993).

3.3 Summary of the Single Slice Experiments

The fundamental conclusion from our investigation of the effect of high ocean wavenumber variability on single-slice inversions is that resolution of this variability from single slice data, even with a long vertical array, is limited by linearization errors. The high ocean wavenumber resolution that is in principle available from tomographic measurements, as discussed by Cornuelle and Howe (1987), is therefore achievable only under restricted conditions. The travel time variability due to these scales is significant and measurable, however, and must therefore be treated as an error source if not explicitly modeled.

It was found that the correct sound speed field could be obtained from the measured travel times using historical data (Levitus) as the starting reference state and iterating.

The effect of internal waves, while fairly well understood for the early well-resolved rays, is still not understood for near-axial and axial arrivals. Work is still in progress on a quantitative comparison between predictions and measurements of internal wave variability.

If another single slice experiment is performed, the following at a minimum should be done: the hydrophone spacing should be much closer than in Slice89, to resolve short spatial scale variability; the transmission schedule should be such that high frequency fluctuations are resolved; the transmissions should be reciprocal (i.e., there should be an acoustic source at both ends of the slice), to understand the effect of ocean currents (internal wave and other scales) on the propagation; lastly, the environmental sampling should be much more dense to sample the loop harmonic wavenumbers.

It was found that MFP is very sensitive to the mean profile, which in hindsight should have been expected. Other tomography work (Dushaw et al., 1993) showed that the UNESCO (internationally accepted) sound speed equation based on the work of Chen and Millero was incorrect; the Del Grosso equation is closer to the truth. The signal gain degradation (SGD) obtained using tomographically generated sound speed fields compared well with those using just the in situ profile data, in some cases.

Additional information is available in Worcester et al. (1994), Cornuelle et al. (1993), and Howe et al. (1991a).

4. MOVING SHIP TOMOGRAPHY

Moving Ship Tomography (MST) as a method of obtaining high resolution, nearly synoptic three-dimensional maps of the ocean interior over large areas was first suggested by Munk and Wunsch (1982) and was explored in detail by Cornuelle et al. (1989). The basic idea is to measure acoustic travel times along a multitude of paths crossing at many different angles and then from these data reconstruct the sound speed (temperature) field in a manner analogous to a medical CAT-scan. To generate a sufficient number of crossing ray paths, a moving receiver is used. From these data, sound speed maps can be reconstructed. Given such maps we will be able to study advecting fronts and interacting eddies with high spatial resolution and test how well numerical models can predict the evolving fields.

All the previous work in ocean acoustic tomography has been done with fixed or moored instruments. The arrays were quite sparse in the horizontal (for a review, see Worcester et al., 1991). The idea of using a moving instrument—whether it be a source, receiver, or transceiver—to improve spatial resolution is by no means new; it is common in seismology, borehole tomography, and medical CAT scanning. Satellite data are starting to be used for ionospheric tomography and to infer atmospheric water vapor tomographically.

The MST experiment discussed here is part of the Acoustic Mid-Ocean Dynamics Experiment (AMODE), the goals of which are

1. Determine the precision with which the ocean mesoscale sound speed (temperature) field can be measured in practice using the technique of Moving Ship Tomography.

2. Study mesoscale eddy kinematics and dynamics. This will include a better determination and understanding of the frequency-wavenumber spectrum, numerical model verification, and data assimilation.

3. Measure gyre-scale variability. Understand how the density, current, and vorticity fields at low wavenumbers (inter-mooring spacing) evolve in time. Determine the effects integral constraints (tomographic measurements) have on eddy-resolving numerical models.

The second and third points will have a direct influence on the ultimate precision of the final four-dimensional (x,y,z,t) field estimates.

We first present theoretical work and simulations done to better understand the MST concept, then discuss early engineering tests, and finally describe the AMODE-MST experiment and results.

4.1 Preliminary Theoretical Work

The first simulations of the MST scenario were discussed by Cornuelle et al. (1989), Figure 22. It was during this work that the full implications of the projection slice theorem became obvious: one needed many crossing ray paths to get the desired horizontal resolution. Using a pair of ships was not sufficient because an inordinate amount of time would be required, during which the ocean would change considerably; a scenario combining (many) fixed instruments with a moving one does give the desired resolution. By trial and error a geometry with six fixed instruments (a pentagon with one in the center) was arrived at. The trade-offs between position errors and mapping errors were investigated; the position error should be less than the equivalent internal wave noise, typically ~10 m. The design of the preliminary experiments and the final AMODE-MST experiment was based on these simulations.

4.2 Preliminary Experimental Work

A test was done at the San Clemente Island Underwater Range (SCIUR) in May 1988 to determine how well we could position the hydrophone array absolutely and to check out all the equipment in preparation for the Greenland Sea work (next paragraph). For this test we tracked the ship and the suspended receiving array with GPS and an ultra-short-baseline acoustic tracking system, respectively. The Range tracked synchronized pingers on the ship and the array. Differences in absolute position were less than 10 m, adequate for MST purposes (see Howe et al., 1989a, for details).

Because a short baseline system tied to the ship depends on the ship's gyrocompass (and also on a vertical reference unit (VRU) to obtain roll and pitch) large absolute errors can be incurred if the gyrocompass is not calibrated or if it is operating in polar latitudes. For this reason, we developed a complementary floating long-baseline (FLBL) system (also called FAST—floating acoustic-satellite tracking range) which uses pingers mounted on buoys along with GPS receivers (for details see Howe et al., 1989a and 1989b). Although this system was deployed in the Greenland Sea tests, GPS coverage was not adequate to exercise it fully. Not until the AMODE-MST experiment was it used to its fullest extent; both systems proved invaluable.

Two engineering tests were performed in the Greenland Sea to gain experience with the MST equipment: deploying the vertical hydrophone array and performing the precise positioning. These tests made use of a moored tomography array deployed there as part of another experiment. The first test was conducted in September and October 1988 (MST88) and the second in August 1989 (MST89). In both cases the equipment worked fairly well but we were severely hampered by the lack of GPS coverage, which made absolute positioning to the required accuracy (10 m) impossible (LORAN has 100 m or larger errors in the area). A significant advance in acoustic signal processing was demonstrated by removing the effects of Doppler shifts due to source/receiver motion. More information can be found in cruise and data reports (Bader et al., 1991; Howe et al., 1991; Worcester and Dushaw, 1993; Worcester and Howe, 1991b).

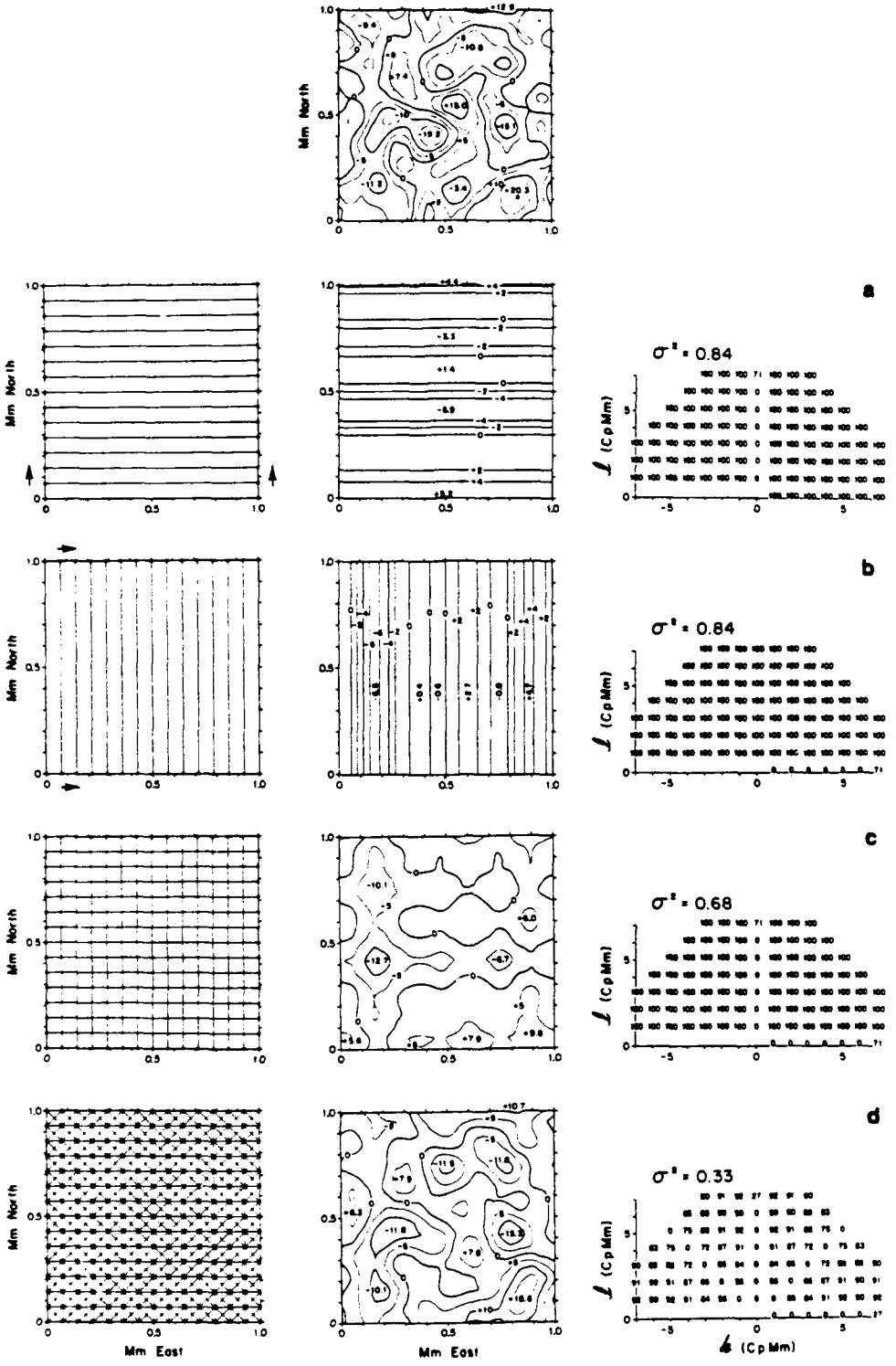

Figure 22. Constructing an image of the ocean using MST. The top center panel is a reproduction of the true ocean which is to be reconstructed by the tomographic inversions. (a) W → E transmissions between the two northward traveling ships (left panel). Inversions of the travel time perturbations produce east-west contours in δC (middle) and only a faint relation to the "true ocean." Residual error variances in wavenumber space (right) are 100% (no skill) except for (k,l) = (0,1),(0,2),...(0,7), which accounts for 16% of the δC variance, leaving σ^2 = 84% overall residual variance. (b) S → N transmissions between two eastward traveling ships. (c) Combined W → E and S → N transmissions, accounting for 32% of the δC variance and giving a slight pattern resemblance to the true ocean. (d) Combined W → E, S → N, SW → NE, and SE → NW transmissions, accounting for 67% of the variance and giving some resemblance to the true ocean.

4.3 The AMODE-MST Experiment

Six acoustic transceiver moorings were deployed between Bermuda and Puerto Rico in March 1991 and recovered a year later (Figure 23). Five moorings were at the vertices of a pentagon on a circle of radius 350 km, and the sixth mooring was at the center (25°N, 66.25°W). The ship circumnavigated the array at a radius of 500 km a little more than two times over a span of 51 days in June and July. A receiving array with a CTD was lowered to 1 km depth every 3 hours approximately every 25 km around the circle. Because of the geometry of the source and (moving) receiver locations, and because the source transmissions were nearly simultaneous, overlapping signals were unavoidable. Special signal processing techniques were developed to improve the signal-to-noise ratio 10–20 dB. Thus, 6 horizontal paths were obtained for each ship stop, producing a total of 750 horizontal crossing paths with a nominal 125 stops around the circle. Each horizontal path typically had 15 identifiable acoustic ray multipath arrivals from which vertical resolution is obtained; so one circumnavigation resulted in roughly 10^4 travel time data which are to a large degree independent. Preliminary results from the experiment have been reported by the AMODE-MST Group (1994).

Travel time perturbations (measured travel time minus predicted travel time from ray tracing through the reference field) for each of the travel time data were calculated. About half the total variance of *0.083 s rms* is due to changes in the ocean, while the other half is due to positioning errors. There are a large number of rays with upper turning points evenly distributed, providing good vertical resolution.

The perturbation travel time data were inverted using standard oceanographic objective mapping techniques to produce fields of perturbation sound speed. In this area sound speed is primarily a function of temperature (and pressure) and is only weakly a function of salinity. The temperature-salinity relation in this area is monotonic, so one can infer density (and geostrophic velocity) from the sound speed.

The weighted least-squares procedure used to produce the objective maps of sound speed is the same whether the data are acoustic travel times or in situ profiles. Empirical modes are used to model the vertical structure (based on historical CTD data as well as CTD data collected on the mooring deployment and recovery cruises and the MST cruise), and a Fourier series is used to represent horizontal structure. Five of the vertical modes are range dependent (with nine Fourier harmonics) and the remaining 15 are range independent, which results in a total of 1160 ocean model parameters for a 1200 km square domain. The minimum length scale currently resolved is about 65 km.

The rms travel time residual (measured travel time minus predicted travel time through the estimated field) is acceptably small, 0.006 s rms. Some of the variance reduction of course is due to corrections in the receiver positions. Position parameters were solved for as part of the inversion process. The position estimates used here have estimated errors of about 30 m, largely because stand-alone GPS data were used for these

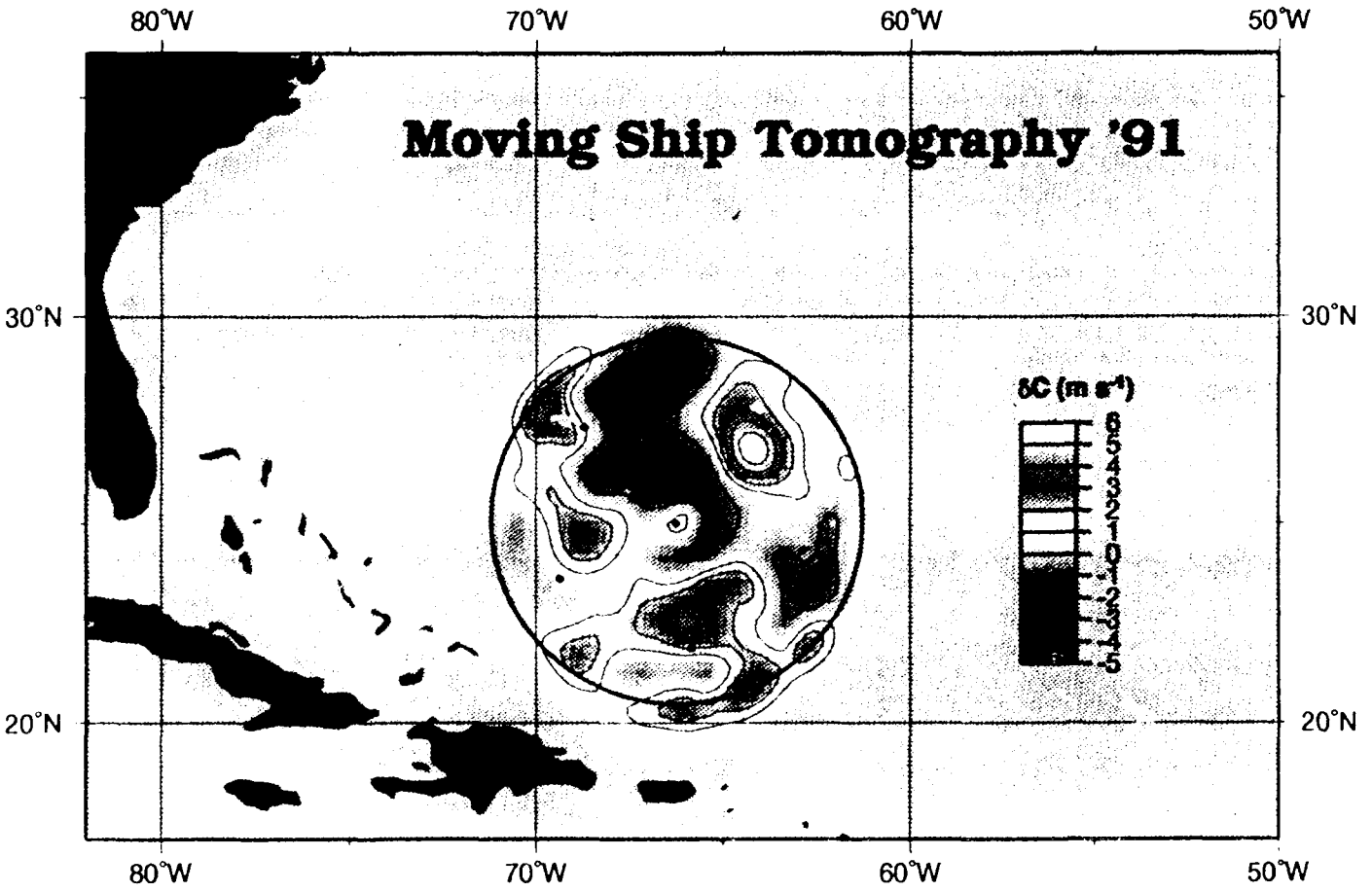

Figure 23 The perturbation sound speed as measured during the Moving Ship Tomography experiment 4-15 July 1991. 1 m/s is equivalent to 0.2°C. The ship with an acoustic receiving array steamed around the 1000-km diameter circle stopping every 3 hours (approximately 25 km) to receive signals from the six moored sources (black dots) The acoustic travel time data were inverted to produce this field

preliminary calculations. Further analysis will be done when the positioning data has been reprocessed using differential GPS data collected on Bermuda, with expected position errors for the subsurface array less than 10 m. This reduction in data error will permit us to increase the spatial resolution of the ocean model and to include dynamics.

Many CTD, XBT, and AXBT profiles were obtained to form an independent data set for comparison purposes (Boyd et al., 1992). The sound speed perturbation field, δC, at a depth of 700 m is shown for the first period (4–18 July) in Figure 23, while that for the second period (15–30 July) is shown in Figure 24 (top left). The horizontal ray paths for the second period are shown in Figure 24 (bottom left). These perturbation maps are remarkable in that they cover such a large area and provide good resolution. Many of the same features are present in each map, which is not entirely unexpected since there is a 7 day overlap in time. The estimated rms perturbation is 2.0 m/s (0.8°C), corresponding to a nominal thermocline displacement of 100 m. The most notable differences between the two maps are that the frontal pattern in the northwest quadrant shifted and the warm eddy in the southwest quadrant split.

The corresponding (standard) error map is in the lower left panel. The uncertainty in the interior is reduced to a nearly uniform 0.6 m/s (0.2°C); the area on the northeast edge has larger uncertainty because of missing data. Outside the circle, the uncertainty rises to a background value (2.0 m/s) nearly that of the *a priori* state (2.2 m/s), the difference being that the acoustic data have reduced the uncertainty in the mean over the whole domain.

On the right side of Figure 24 are the corresponding perturbation and error maps obtained using only the 700 m data from the AXBT profiles taken between 19 and 22 July. The locations of the AXBT casts are shown on the bottom right. These fields are independent of the acoustic data. Perturbations show up only in the vicinity of the AXBT data, and the perturbation field there is very similar to the one obtained from only the acoustic data. The uncertainty field clearly shows the local nature of the profile data and the length scales in this particular parameterization of the ocean. The average uncertainty where there are profiles is 0.8 m/s.

A rigorous comparison must take into account the uncertainty of each estimate. The average difference of the two estimates divided by the estimated uncertainty of the difference is 1.0 standard deviation within the AXBT domain; there is one small spot at 26°N, 69°W where the weighted difference reaches 3 standard deviations; this is not unexpected given that there is a front there and that it is most likely advecting during the 15 days it took to make the acoustic map.

The preceding paragraphs discussed the sound speed at 700 m over the entire area. Now we extract the vertical slice of sound speed perturbation along the MST circle, starting at the northernmost point and going clockwise, Figure 25. The top panel shows the result using only CTD data (taken on the MST circle); the lower one shows the result

of using only acoustic data. The qualitative agreement is good. The differences can be attributed to (at least) two factors, errors and gaps in each data set, and the finite sampling time.

The rms sound speed perturbation averaged over all the CTD data (the measured CTD data relative to the Levitus reference state) peaks at about 2.2 m/s in the main thermocline, Figure 26. The rms difference between the measured CTD sound speed and the sound speed estimated using only acoustic data is about 0.8 m/s, the same as the rms difference between the mapped and measured CTD data. The total rms *a priori* uncertainty was 2.4 m/s at 700 m and included uncertainty in the mean profile. The corresponding variance reduction from the *a priori* value is 94%. The uncertainty near the surface is large (as can be seen in Figure 25) because all the acoustic rays converge at the receiver at 1000 m depth and do not sample the upper ocean in the vicinity of the receiver.

4.4 Summary of Moving Ship Tomography

These results show that using a moving receiver to obtain high-resolution, three-dimensional maps of the ocean sound speed field works in practice. This extension of the original concept of moored ocean acoustic tomography adds a powerful new technique to those available to map ocean structure over large areas. The method can be extended to measure absolute water velocity by adding an acoustic source to the ship array and measuring reciprocal travel times. Depending on the particular interest, one can imagine experiments ranging in scale from kilometers to full ocean basins.

There is much yet to be done with this very rich data set. There is an obvious need for dynamical models to interpolate in time and space, combining various types of data in a consistent way. We attribute the differences between the fields determined from profile measurements and those from the tomographic measurements to the change in the fields during the finite sampling times. The first step is to use a nonlinear quasi-geostrophic model in a Kalman filter to assimilate the tomographic and other data as a function of time. This effort is currently in progress. The next step is to do a model verification study; i.e., given the initial field in June, can the model predict the field in July? Using a dynamical model for data assimilation makes no sense unless the model is correct. Finally, we will study the value of integral constraints on eddy-resolving numerical ocean models. What is the minimum amount of tomographic data needed to keep the fields produced by a dynamical model sufficiently close to those in the real ocean to be useful for making acoustic predictions?

There is also an obvious need to improve our knowledge of the frequency-wavenumber spectrum of ocean sound speed (thermal) variability, covering temporal and spatial scales from internal waves to the gyre. This is the environment in which any acoustic signal processing algorithm must work. The tomographic and other data obtained in the AMODE-MST experiment will improve our statistical description of

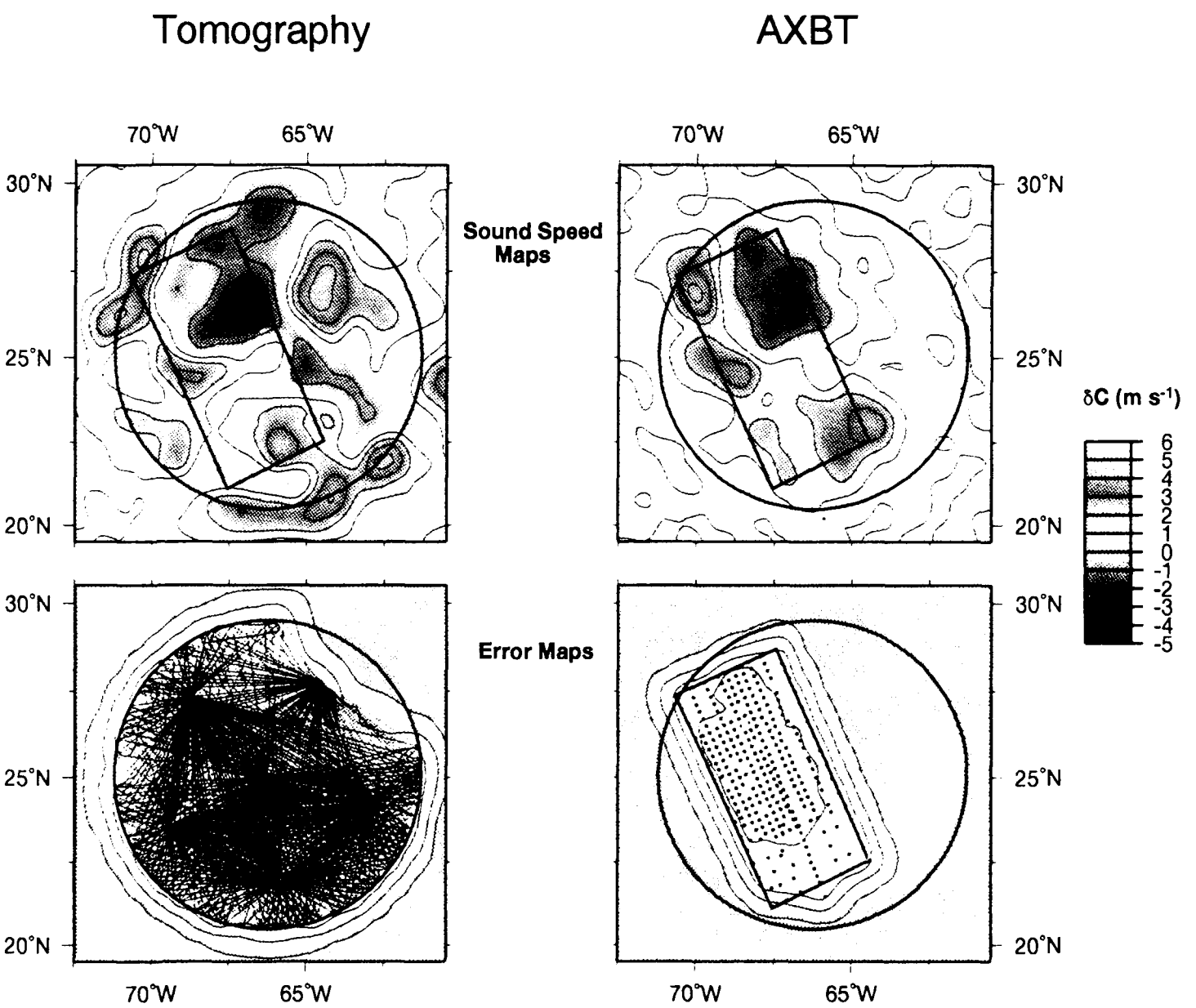

Figure 24 Perturbation sound speed, δC, and estimated rms uncertainty at 700 m. The maps in the left column are obtained using only acoustic data (15-30 July) while the maps in the right column are obtained using only AXBT data at 700 m (18-22 July). The horizontal acoustic ray paths sampled are shown on the lower left map; the locations of the AXBT profiles are shown on the lower right map. The contour intervals are 1 m/s for the perturbation maps (top) and 0.5 m/s for the uncertainty maps (bottom).

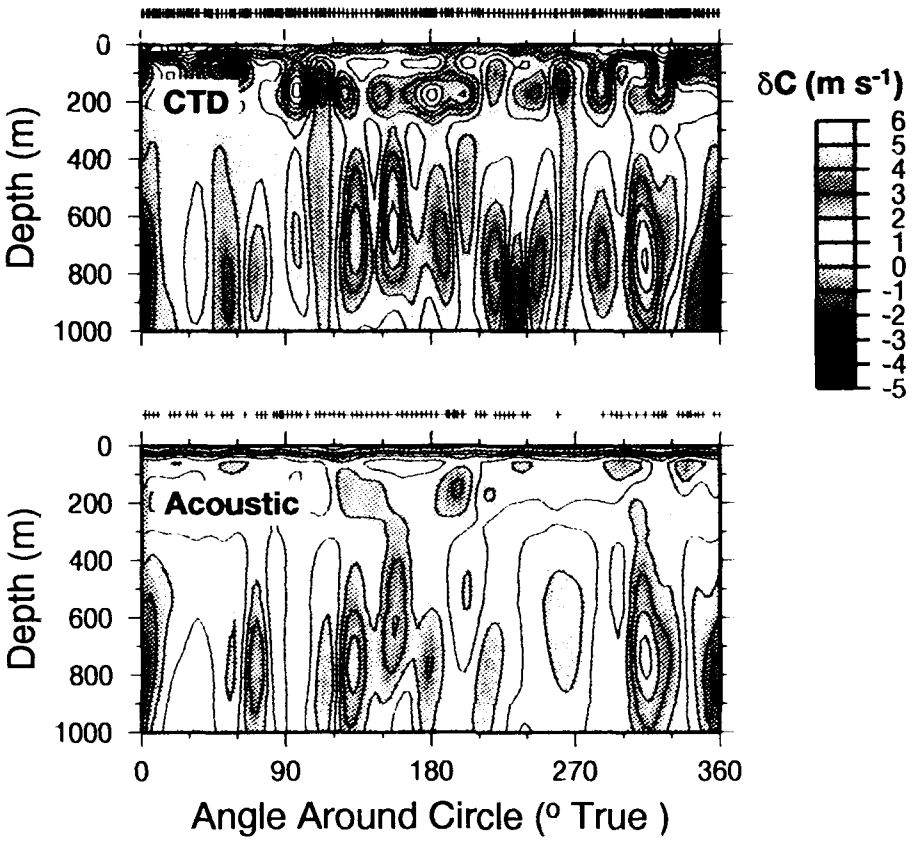

Figure 25. Sound speed perturbation, δC, as a function of depth and angle around the MST circle (starting at the northernmost point and going clockwise with a radius of 500 km; the total length of the section is 1000 π km). The top panel shows the field obtained using only CTD profile data, and the bottom panel shows the field obtained using only acoustic data during the same time period, 4-15 July. The locations where CTD and acoustic data were obtained are marked.

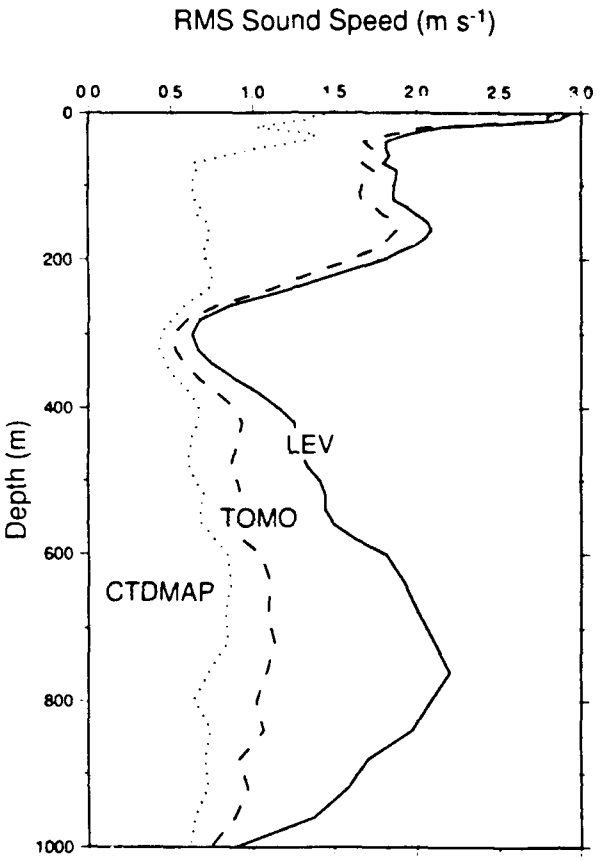

Figure 26. Profiles of a priori and a posteriori rms uncertainty and rms difference (tomography minus profile).

ocean variability. In particular, the data collected will provide significant information on internal tides. Preliminary results from a recent Pacific experiment indicate that internal tides may have significant correlation scales and therefore affect acoustic propagation more than has been previously appreciated.

The sound speed field determined from in situ profile measurements and the sound speed field determined from moving ship tomography give essentially identical matched field processing results (R. Heitmeyer, personal communication).

5. CONCLUSIONS AND RECOMMENDATIONS

We first list specific conclusions from each experiment before giving more general conclusions and recommendations.

SLICE89. This experiment was the first to show acoustic wavefronts over a large part of the water column. The major remaining unresolved acoustic propagation problem is to understand the effect of internal waves on the last second or so of the arrival pattern. We expect that the simulations and theory being worked on by Colosi and Flatté will begin to unravel this mystery. The key conclusions are

1. The overall measured wavefront pattern is well predicted. Discrepancies, however, are present in the last second of the pattern in two ways. First, there is more energy in the off-axial final arrivals than predicted, and second, fewer rays can be resolved than expected. Simulations with explicit internal wave fields can account for part of these discrepancies (Flatté, 1993; Colosi et al., 1994). There is also a suggestion that the axial cutoff arrives later than predicted. The axial final cutoff time is only marginally consistent with predictions made using the measured sound speed field. Further work to investigate this discrepancy is required, however, since the near-axial sound speed field was not well measured in this experiment.

2. It will be difficult to obtain high oceanic wavenumber information tomographically in a stand-alone single slice experiment because of a relatively large degree of nonlinearity. If, however, there are slices embedded within a mapping experiment (such as AMODE-MST), it may be possible to obtain useful resolution at high wavenumbers.

3. It was found that the correct mean sound speed profile could be obtained from the measured travel times using historical data (Levitus) as the starting reference state and iterating. Thus, at least for the circumstances of this experiment, no in situ environmental data are necessary.

4. Matched field results were very sensitive to the mean sound speed profile. Results using the tomographically determined sound speed field were similar to those obtained using the sound speed field determined from in situ profile measurements. The internal wave results and the tomographic results further quantify the "noise" for matched field processing; the latter must be robust against internal wave noise, as well as the unresolved high wavenumber ocean variability.

AMODE-MST. This experiment showed that a moving tomography receiver can greatly augment a fixed array of transceivers. In the future, it should be possible to use a moving transceiver to obtain absolute water velocity, which should be a strong constraint

on a model. Operationally, one would not expect such a contrived geometry as in this experiment. Rather, there would most likely be a few fixed sources in an ocean basin, perhaps as part of the ATOC program (Acoustic Thermometry of Ocean Climate), a few LFA (low frequency active) moving sources, and quite a few moving receivers (ships or drifters), in addition to fixed Navy and civilian receivers. All the relevant data would be sent to FNOC, combined with other data types, and assimilated into a numerical circulation model to produce an optimal nowcast and forecast of the ocean sound speed field. The main conclusions are

1. Sound speed fields determined tomographically and those determined using in situ profile data agree within the uncertainty of each. This demonstrates that the tomographic technique can measure large volumes of the ocean with high resolution and is a practical alternative to other methods.

2. The matched field results based on tomographic sound speed fields and on in situ sound speed fields from profilers were essentially identical.

We now give some general conclusions and recommendations.

1. It is essential that ALL data (in situ, tomographic, satellite, etc.) be combined with an ocean numerical model to produce an optimal estimate of the ocean state (Figure 27). There will most likely never be enough data of any single kind to fully determine the ocean. The physics of the model should provide the framework to combine the different data types, and the interpolation in time and space, and the data should constrain the model (with imperfect physics) so it does not wander from the truth. Future experiments could obtain standard Navy products, available from FNOC, but arrange to supplement the input data as needed for the particular experiment.

2. The question *How well does one need to know the sound speed field for the purposes of matched field processing?* has not yet been answered. The question is a difficult one, in that the answer almost certainly cannot be specified in terms of the required sound speed uncertainty at all points. Rather, acoustic propagation calculations depend on specific averages of the sound speed field, and it is the precision with which these averages are measured that is important. Which moments of the sound speed field are important depends on the propagation code used. One of the first order tasks remaining is therefore careful comparisons of measured and predicted arrival patterns using various propagation codes (e.g., adiabatic normal modes, coupled normal modes, etc.) to determine which codes provide sufficiently accurate predictions for matched field processing algorithms.

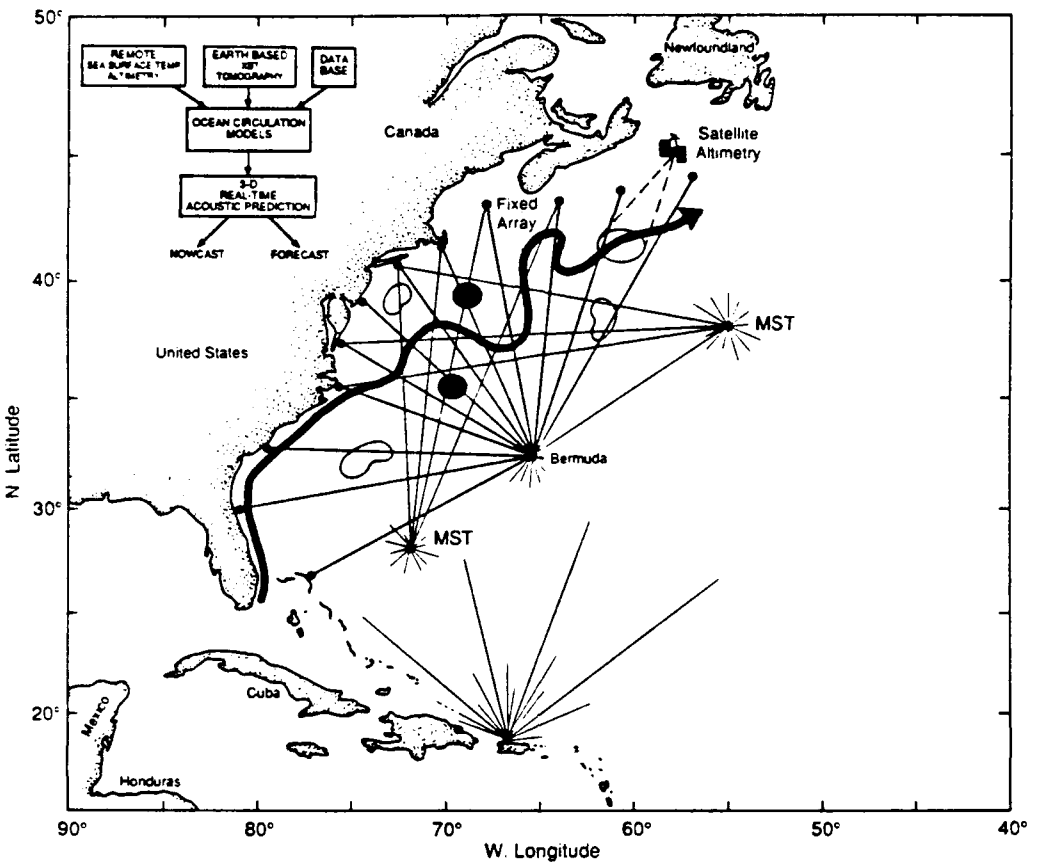

Figure 27. All available assets are employed to collect acoustic data, which are used with all other possible complementary data to provide ocean nowcasts and forecasts.

REFERENCES

AMODE-MST Group: T.G. Birdsall, J. Boyd, B.D. Cornuelle, B.M. Howe, R. Knox, J.A. Mercer, K. Metzger, Jr., R.C. Spindel, and P.F. Worcester, Moving ship tomography in the northwest Atlantic Ocean, *Eos, 75,* 17, 21, and 23, 1994.

Bader, C.M., B.M. Howe, J.A. Mercer, P.F. Worcester, B.D. Cornuelle, and J. Lynch, CTD, XBT, and XSV Data from the Greenland Sea: R/V Knorr Cruise 8809 (6 September – 4 October 1988) and R/V Endeavor Cruise EN200 (3 August – 10 September 1989) (Department of State Cruises 88-18 and 88-120), APL-UW TM3-91, Applied Physics Laboratory, University of Washington, 1991.

Boyd, J.D., J.D. Lavoie, R.K. Myrick, and R.S. Linzell, Environmental Data Catalog: MDA-91, June-July 1991, NOARL Tech. Note 225, February 1992.

Colosi, J., The nature of wavefront fluctuations induced by internal gravity waves in long-range oceanic acoustic pulse transmissions, Ph.D. thesis, University of California, San Diego, 1993.

Colosi, J.A., S.M. Flatté, and C. Bracher, Internal-wave effects on 1000-km ocean acoustic pulse propagation: Simulation and comparison with experiment, *J. Acoust. Soc. Am.*, submitted 1994.

Cornuelle, B.D., and B.M. Howe, High spatial resolution in vertical slice ocean acoustic tomography, *J. Geophys. Res.*, *92*, 11,680–11,692, 1987.

Cornuelle, B.D., W.H. Munk, and P.F. Worcester, Acoustic tomography from ships, *J. Geophys. Res.*, *94*, 6232–6250, 1989.

Cornuelle, B.D., P.F. Worcester, J.A. Hildebrand, W.S. Hodgkiss, Jr., T.F. Duda, J. Boyd, B.M. Howe, J.A. Mercer, and R.C. Spindel, Ocean acoustic tomography at 1000-km range using wavefronts measured with a large aperture vertical array, *J. Geophys. Res.*, *98*, 16,365–16,377, 1993.

Duda, T.F., S.M. Flatté, J.A. Colosi, B.D. Cornuelle, J.A. Hildebrand, W.S. Hodgkiss, Jr., P.F. Worcester, B.M. Howe, J.A. Mercer, and R.C. Spindel, Measured wavefront fluctuations in 1000-km pulse propagation in the Pacific Ocean, *J. Acoust. Soc. Am.*, *92*, 939–955, 1992.

Dushaw, B.D., P.F. Worcester, B.D. Cornuelle, and B.M. Howe, On equations for the speed of sound in seawater, *J. Acoust. Soc. Am.*, *93*, 255–275, 1993.

Flatté, S.M., Random-media effects in ocean acoustics: An introduction, in *Wave Propagation and Random Media (Scintillation)*, SPIE Press and Institute of Physics Publishing, in press, 1993.

Howe, B.M., P.F. Worcester, and R.C. Spindel, Ocean acoustic tomography: Mesoscale velocity, *J. Geophys. Res.*, *92*, 3785–3805, 1987.

Howe, B.M., J.A. Mercer. R.C. Spindel, and P.F. Worcester, Accurate positioning for moving ship tomography, OCEANS'89, *3*, 880–886, 1989a.

Howe, B.M., J.A. Mercer, and R.C. Spindel, A floating acoustic-satellite tracking (FAST) range, in *Proc. MDS '89: Conference and exposition on marine data systems*, Marine Technology Society, 1989b.

Howe, B.M., J.A. Mercer, R.C. Spindel, P.F. Worcester, J.A. Hildebrand, W.S. Hodgkiss, Jr., T.F. Duda, and S.M. Flatté, SLICE89: A single slice tomography experiment, in *Ocean Variability and Acoustic Propagation*, J. Potter and A. Warn-Varnas, eds., Kluwer, Dordrecht, the Netherlands, 81–86, 1991a.

Howe, B.M., B.D. Cornuelle, J.A. Mercer, K. Metzger, and P.F. Worcester, Acoustic Mid-Ocean Dynamics Experiment: 1991 Moving Ship Tomography Cruise, APL-UW TM 18-91, Applied Physics Laboratory, University of Washington, 1991b.

Kak, A.C., and M. Slaney, *Principles of Computerized Tomographic Imaging*, IEEE Press, New York, 1988.

Levitus, S., Climatological Atlas of the World Ocean, NOAA Professional Paper 13, 173 pp., 1982.

Lynn, R.J., The subarctic and northern subtropical fronts in the eastern North Pacific Ocean in spring, *J. Phys. Oceanogr.*, *16*, 209–222, 1986.

Munk, W., and C. Wunsch, Ocean acoustic tomography: A scheme for large-scale monitoring, *Deep-Sea Res.*, *26*, 123–161, 1979.

Munk, W., and C. Wunsch, Observing the ocean in the 1990s, *Phil. Trans. R. Soc. Lond. A*, *307*, 439–464, 1982.

Sparrock, R.C., Stability of time fronts on a large vertical array at long range in the ocean, Masters thesis, University of California, San Diego, 1990.

Worcester, P.F., and B.D. Dushaw, The Acoustic Mid-Ocean Dynamics Experiment: Recovery Cruise Report, Scripps Institution of Oceanography Reference Series 93-8, 1993.

Worcester, P.F., and B.M. Howe, The Acoustic Mid-Ocean Dynamics Experiment: Cruise report of AMODE Deployment, Applied Physics Laboratory, University of Washington, April 1991.

Worcester, P.F., B.D. Cornuelle, and R.C. Spindel, A review of ocean acoustic tomography: 1987–1990, *Reviews of Geophysics*, Suppl., 557–570, 1991.

Worcester, P.F., B.D. Cornuelle, J.A. Hildebrand, W.S. Hodgkiss, Jr., T.F. Duda, J. Boyd, B.M. Howe, J.A. Mercer, and R.C. Spindel, A comparison of measured and predicted broadband acoustic arrival patterns in travel time-depth coordinates at 1000-km range, *J. Acoust. Soc. Am.*, *95*, 3118–3128, 1994.

REPORT DOCUMENTATION PAGE

Form Approved
OPM No. 0704-0188

1. AGENCY USE ONLY *(Leave blank)*	2. REPORT DATE	3. REPORT TYPE AND DATES COVERED
	July 1994	Technical

4. TITLE AND SUBTITLE

Ocean Acoustic Tomography: Single Slice and Moving Ship Experiments

5. FUNDING NUMBERS

N00014-87-K-0760
N00014-87-K-0120
N00014-91-J-4055
N00014-91-J-4117
N00039-91-C-0072

6. AUTHOR(S)

Bruce M. Howe and Peter F. Worcester

7. PERFORMING ORGANIZATION NAME(S) AND ADDRESS(ES)

Applied Physics Laboratory
University of Washington
1013 NE 40th Street
Seattle, WA 98105-6698

8. PERFORMING ORGANIZATION REPORT NUMBER

APL–UW TR 9308

9. SPONSORING / MONITORING AGENCY NAME(S) AND ADDRESS(ES)

Dr. Richard Doolittle, Code 321SS
Office of Naval Research
Ballston Towers #1
800 N. Quincy Street
Arlington, VA 22217-5500

10. SPONSORING / MONITORING AGENCY REPORT NUMBER

11. SUPPLEMENTARY NOTES

12a. DISTRIBUTION / AVAILABILITY STATEMENT

Approved for public release; distribution is unlimited.

12b. DISTRIBUTION CODE

13. ABSTRACT *(Maximum 200 words)*

The results of the ocean acoustic tomography work that supported the development of matched field processing (MFP) are summarized. This report focuses on two experiments. In Slice89 a single source transmitted to a vertical hydrophone array. This experiment improved our understanding of the single slice transfer function from scales of internal waves to 1000 km. It demonstrated the importance of unresolved high wavenumber ocean mesoscale variability to acoustic propagation. Any coherent signal processing technique must be robust against both internal wave variability and unresolved high wavenumber mesoscale variability, as both contribute roughly comparable amounts of travel time variance. The Acoustic Mid-Ocean Dynamics Experiment - Moving Ship Tomography Experiment (AMODE-MST) was a large mapping effort to address the primary goal of this tomography effort — to determine the precision with which the ocean mesoscale sound speed field can be measured for input into matched field (or other) processing of long-range acoustic transmissions. The experiment demonstrated that tomographic techniques can be used to measure the sound speed structure over a large area with high resolution.

14. SUBJECT TERMS

Ocean acoustic tomography, mesoscale oceanography, coherent signal processing, ocean acoustics, acoustic propagation

15. NUMBER OF PAGES

53

16. PRICE CODE

17. SECURITY CLASSIFICATION OF REPORT	18. SECURITY CLASSIFICATION OF THIS PAGE	19. SECURITY CLASSIFICATION OF ABSTRACT	20. LIMITATION OF ABSTRACT
Unclassified	Unclassified	Unclassified	SAR